DYNAMIC PLASTIC BEHAVIOR OF INTERSECTING SHELLS

by

Kipling Edward Grassit

DYNAMIC PLASTIC BEHAVIOR
OF INTERSECTING SHELLS

by

KIPLING EDWARD GRASSIT
B.S., UNITED STATES COAST GUARD ACADEMY
(1965)

SUBMITTED IN PARTIAL FULFILLMENT
OF THE REQUIREMENTS FOR THE
DEGREE OF NAVAL ENGINEER
AND THE DEGREE OF
MASTER OF SCIENCE IN MECHANICAL ENGINEERING
at the
MASSACHUSETTS INSTITUTE OF TECHNOLOGY
JUNE, 1971

DYNAMIC PLASTIC BEHAVIOR OF INTERSECTING SHELLS

by

KIPLING EDWARD GRASSIT

Submitted to the Department of Naval Architecture and Marine Engineering and the Department of Mechanical Engineering on May 14, 1971, in partial fulfillment of the requirements for the degree of Naval Engineer and the degree of Master of Science in Mechanical Engineering.

ABSTRACT

Presented herein are the results of a series of tests made to determine the permanent deformations of intersecting spherical and cylindrical shells fully clamped around the base of the sphere and subjected to uniformly distributed impulsive loads. The specimens were made from 6061-T6 aluminum. In addition, tests were conducted on cylindrical panels made from 6061-T6 aluminum and hot-rolled mild steel. It is concluded that strain-rate sensitivity of the material is important. It is also concluded that the cylindrical nozzle has the effect of reducing the permanent deflections in the sphere of the intersecting sphere-cylindrical nozzle.

Thesis Supervisor: Norman Jones

Title: Associate Professor of Naval Architecture

ACKNOWLEDGEMENTS

The author owes a special debt of gratitude to Professor Norman Jones, his thesis supervisor, without whose advice and support this report could not have been done. The author wishes to thank the Coast Guard Research and Development Branch for their financial support and Cdr. Coburn for his assistance in obtaining it. A special thanks goes to Mary Ann, the author's wife, for her patience and encouragement, and for typing the report.

TABLE OF CONTENTS

TABLE OF CONTENTS (Continued)

LIST OF TABLES

SECTION I

SECTION II

APPENDICES

Section A

LIST OF TABLES (Continued)

Section B

LIST OF FIGURES

INTRODUCTION

Today, a wide range of materials used in many complex structures are required to perform to the limits of their mechanical strength and endurance. It is often desirable to be able to predict the maximum dynamic energy a structure can absorb before failure, or to be able to predict the deformations that result from a collision with another body or from being subjected to explosive loads. Designs utilizing plasticity theory are often more realistic in their predictions than those using elastic methods alone.

Analysis of the plastic behavior of structures is often simplified by disregarding any elastic deformations when the structure is statically loaded. This rigid-plastic method of analysis has been shown by experimentation on a variety of structures to be generally valid under static loading conditions.

The rigid-plastic methods developed for statically loaded structures have been extended to dynamic loading situations in order to predict their behavior under these conditions. Symonds (29) has indicated that these predictions are reasonable when the external dynamic energy imparted to a structure is at least ten times the amount of energy which could be absorbed elastically by the structure, and in addition to this, the load duration

should be short compared to the natural period of the structure.

Elementary rigid-plastic theory neglects elastic effects, strain hardening, strain-rate sensitivity, and geometry changes. The validity of these assumptions have been subjected to numerous investigations.

Cylindrical shells have been investigated by Hodge (11, 12, 14) and others (8,22) using various boundary conditions and dynamic loads. These theoretical analyses, however, disregard geometry changes and the influence of strain-rate sensitivity.

Jones (20) analyzed cylindrical shells and concluded that in the dynamic case, geometry changes are important even for small deflections and should be retained in cylindrical shell analysis with axial constraints.

Baker (1) developed a theory for the elastic-plastic response of thin spherical shells subjected to spherically symmetric internal transient pressure loads. His analysis includes the effects of strain hardening but neglects strain-rate sensitivity of the shell material.

Wierzbicki (31) presented a solution for a spherical container neglecting strain hardening but includes strain-rate sensitivity. He showed that impulsive loading of a spherical container may lead to large strain-rates, and concludes that strain-rate sensitivity of the material must be retained in the analysis. He stated that no simple

function describing the influence of strain-rate can closely approximate the real behavior of the material over a wide range of strain-rates. He also showed that if strain-rate is accounted for, the magnitude of the final strain depends upon the shape of the impulse and depending on this shape, the magnitude of the final strain can be either smaller or larger than those predicted by a rigid, perfectly - plastic solution.

Most experimental investigations have been conducted on such structures as beams, cantilevers, and plates. Parkes (26) subjected mild steel beams to dynamic loads and found that the permanent deformations that resulted were smaller than those predicted by rigid-plastic theory. Tests on cantilever beams conducted by Bodner and Symonds (2) showed that strain-rate sensitivity was important. Recent experimental work by Jones, et al, (16,17) has shown that geometry changes and strain-rate sensitivity of the material are important. These have shown that the predictions made by rigid-plastic theories are acceptable provided that the influence of geometry changes is retained for moderate deflections as well as strain-rate sensitivity when appropriate. Jones (18,19) has shown that strain-rate sensitivity is generally more important than strain hardening of the material.

Giannotti (10) subjected spherical caps to impulsive loads and concluded that strain-rate sensitivity is an

important consideration. He also observed that the effect of strain hardening was negligible.

As far as this author is aware, no theoretical, or experimental investigations have been published on spherical shells intersected by a cylindrical nozzle subjected to dynamic loads sufficient to cause plastic flow of the material. However, Jones (21) has presented a tentative method of approximating deflections for the sphere-nozzle intersection. This method neglects geometry changes and strain-rate sensitivity as well as assumes that the material is rigid, perfectly plastic.

The author presents the results of five tests conducted on spherical shells intersected axisymmetrically by a cylindrical nozzle subjected to uniformly distributed internal impulsive loads.

The spherical shell is a hemisphere and is rigidly clamped around its base, while the cylindrical nozzle is not constrained. The shells were made from 6061-T6 aluminum which is relatively insensitive to strain-rate. These tests are presented in Section I.

In addition, twelve tests were conducted on 90-degree cylindrical shell panels which were subjected to a uniformly distributed impulse sufficient to cause plastic deformation of the panel. These panels were made from hot-rolled mild steel and 6061-T6 aluminum. Since mild steel is a strain-rate sensitive material and 6061-T6

aluminum is not, a comparison of results allows the influence of strain-rate sensitivity to be estimated. These tests are a continuation of the work conducted by Dumas (6), and are presented in Section II.

It is hoped that the results presented here may aid in assessing such numerical procedures as developed by Leech, Witmer, and Pian (23) and in developing approximate or exact methods of analysis such as those presently being undertaken in the Department of Naval Architecture and Marine Engineering at Massachusetts Institute of Technology.

SECTION I

TESTS ON INTERSECTING SPHERICAL AND CYLINDRICAL SHELLS

NOTATION

D	Mean diameter
H	Wall Thickness
R	Mean radius
L	Length of nozzle (outside)
I	Total impulse $I = I_o W_e$
I_o	Specific impulse
M	Mass of specimen acted on by initial velocity V
V	Initial velocity $V = I/M$
W	Permanent deflection
W^*	Average permanent deflection near the sphere-nozzle intersection (point "C", or "G" of figure 5)
W_{fn}	Average permanent deflection at nozzle free-end.
W_e	Weight of explosive
λ	Impulse parameter $\lambda = \dfrac{\rho V^2 R^2}{\sigma_o H^2}$
ρ	Mass density of material
σ_o	Yield stress of material in simple tension

Subscripts n, and s refer to cylindrical nozzle and sphere of each specimen respectively.

EXPERIMENTAL DETAILS

DuPont "Detasheet" explosive in a range of thickness from 0.010 inches to 0.015 inches was applied over the inner surface of each intersecting shell test specimen. A 1/4 inch thick layer of low density (0.027 gm/cm^3) polyeurethene foam was employed as an attenuator between the sheet explosive and the specimen surface. This explosive - attenuator system was calibrated and found to have a specific impulse of 18.42 x 10^4 dyne-sec/gm or 0.4125 lb-sec/gm (See Appendix B). It was only necessary to weigh the explosive to compute the actual impulse imparted to the specimen in each test. DuPont 6484 cement was used between the "Detasheet", foam and the test specimen.

Each test specimen consisted of a flanged, five inch diameter hemisphere intersected axisymmetrically by a four inch long cylinder with a two inch diameter. The hemisphere had a nominal thickness of 0.111 inches while the nominal thickness of the cylinder was 0.081 inches.

The sphere and cylindrical nozzle thicknesses were designed such that the static collapse pressure would be approximately equal. For the sphere,

$$p_c = \frac{2\sigma_o H_s}{R_s}$$

For the cylindrical nozzle

$$p_c = \frac{\sigma_c H_n}{R_n}$$

Therefore, the thickness of the cylindrical nozzle was adjusted such that

$$H_n = \frac{2 H_s R_n}{R_s}$$

The hemisphere was formed from 6061 aluminum flat plate using a hydroforming process, then machined to provide a more uniform thickness. The cylinder was machined from 6061 aluminum solid round stock. The intersection was made by using a Tungsten Inert Gas (TIG) welding process. A No. 4043 aluminum filler rod with a yield strength of 22,000 psi was used in the weld.

After the welded joint was made, the inside and outside surface of the joint was machined to provide a sharp intersection. After the specimens were fabricated, they were heat treated to the T6 condition. Figure 1 shows a typical specimen.

Figure 4 illustrates the specimen clamping arrangement. The clamps were made of 1/2 inch thick steel plate. The clamping surfaces were serrated and case hardened in an attempt to ensure that the fully clamped support condition, with no slippage of the specimen, would exist. Clamps are shown in figures 2a-c.

Prior to testing, each specimen was measured to obtain its actual dimensions. Thicknesses were measured

using a dial indicator. These measurements are given in Tables I a-e. The coordinate system used for these tables is the same used to measure permanent deflections as shown in figure 5. The observed variation of thickness for all specimens was less than ± 0.0007 inches for the hemisphere, and ± 0.0006 inches for the cylinder. The outside diameter and length of the cylinder was measured using a micrometer and inside caliper.

The outside diameter of the hemisphere was obtained by chucking each specimen on a lathe and adjusting it so that the hemisphere turned on-center. A dial indicator was mounted on the tool post and adjusted to measure on-center, with the dividing head adjusted to move transversely. A reference point was picked near the flanged end and the dividing head and crossfeed adjusted to produce a reference reading on the dial indicator. The dividing head was then moved a given amount and then the crossfeed was adjusted to produce the same reference reading on the dial indicator. A series of such points was obtained for each specimen and are given in Table 2a-e. The coordinate system used for this operation is shown in Figure 7. An average outside diameter was then obtained graphically. Figure 7 shows the plot of a typical specimen.

Initial deflection readings were taken using the apparatus shown in Figure 8. The specimen was then loaded with the foam attenuator and explosive and the

specimen -- clamps arrangement bolted to the metal support table (figure 4). Figure 6 shows the general arrangement of apparatus for tests. A "Detasheet" leader 0.125 - in x 0.010 - in x 20 - in was employed between the explosive sheet and a No. 6 electric blasting cap. The leader was split with one end attached to the explosive in the sphere and the other to the explosive in the cylinder. The leader was attached by simply pressing the end into the sheet explosive with a finger.

The specimen was removed from the clamps and final deflections taken. The permanent deflections caused by the impulse loading was simply the difference between the final and initial deflections obtained. These deflections were measured to the nearest 0.0001 inch. The coordinate grid system used in measuring deflections is shown in Figure 5.

The average density of the 6061-T6 aluminum material for both the hemisphere and cylinder was obtained by carefully weighing several samples and using a water displacement method to measure their volume. The density of the 6061-T6 aluminum was found to be 2.495×10^{-4} $lb\text{-}sec^2/in^4$ for the sphere and 2.479×10^{-4} $lb\text{-}sec^2/in^4$ for the cylindrical nozzle.

Appendix A gives the results of tensile tests conducted on the specimen materials.

Eccentricity between the sphere and nozzle axes was checked and found to be 0.05 inches.

DISCUSSION OF RESULTS

The results for the impulsively loaded sphere-cylindrical nozzle test specimens are given in Tables

Figures 9 and 10 show the deflection parameter W*/H as it varies with the impulse parameter, λ, and the uniformly distributed impulse velocity V.

The deflection parameter W*/H was determined by averaging the deflections at points "C" and "G" of figure 5 for the sphere and nozzle respectively. Average values were chosen due to the non-symmetric deflections obtained in the tests. The reason for the non-symmetric deflections is not fully understood. The author believes that the non-symmetry might be caused by a number of factors.

First, the spherical section of each test specimen is not actually spherical in shape, but is more ellipsoidal. When the spheres were measured for their outside diameter, it was observed that each sphere had a major and minor axes, perpendicular to each other, that varied in length by about 0.015 inches. Eccentricity between the axes of the sphere and nozzle might also contribute to the non-symmetric deflections. Non-homogeneity of the heat affected zone of the welded intersection, or, of the base material itself, might also have contributed to the

non-symmetry of the deflections. The explosive used may, in fact, be non-homogeneous, and therefore, the velocity distribution may not be uniform. The perforation procedure used to reduce the loading impulse may also contribute to a non-uniform velocity distribution.

The deflection profiles using average values are shown in figure 11 a-d.

Figure 9 shows a non-linear relation between W^*/H and λ. This relation, for the sphere, appears to agree with the results obtained on 180 degree spherical caps by Giannotti (10).

Figure 10 appears to show a relative linear relation between W^*/H and V. This relation also agrees with reference (10) for the sphere.

Specimen No. 1 does not fall with the other tests as the explosive loaded into the nozzle failed to detonate. It does show the effect of the nozzle in that the resulting deflections were much smaller than if the nozzle had been subjected to an impulsive load.

No results were obtained in Test No. 5 as the load caused catastrophic failure in the nozzle. The nozzle section was completely sheared in the axial direction at several locations. There were also cracks about one inch long in the sphere that corresponded to the axial failures of the nozzle. The nozzle had separated from the sphere, between the cracks, precisely at the sphere-nozzle

intersection. It is felt that the failures started at defects in the welded intersection joint and propagated into the nozzle and sphere. Tests No. 2, 3, and 4 appear to confirm the assumption that weld defects were the initiation points of the failure in Test No. 5. These tests exhibited very small hairline cracks at the sphere-nozzle intersection. These cracks were also propagating in the axial direction of the nozzle (perpendicular to the sphere-nozzle junction).

These results show that the welded joint is of prime concern in the design of similarly shaped structures that might be subjected to impulsive loads.

In order to obtain better results from experiments of this type, it is recommended that a larger number of test specimens be used. It is recommended that additional tests be conducted, and that these tests should use specimens of greater wall thickness than those used here. This is to eliminate the need for perforating the explosive in order to reduce the impulsive loads. It is also recommended that the diameter of the cylindrical nozzle be reduced and that the tests be conducted by loading the explosive into the sphere only.

By thus changing the experimental procedures, it may be possible to better assess the influence of the intersecting nozzle by comparing results with those obtained by Giannotti (10) for spherical caps.

CONCLUSIONS

An experimental study into the dynamic behavior of intersecting spherical and cylindrical shells fully clamped around the base of the sphere and subjected to uniformily distributed loads is reported. The loads were sufficient to cause plastic flow of the material. The material used for all tests was 6061-T6 aluminum.

Due to the limited number of tests conducted on the sphere-cylindrical nozzle intersections, it is not possible to draw any concrete conclusions as to the influence of the intersection.

However, it is felt that the nozzle has the effect of reducing the maximum deflection that might be obtained for a spherical cap subjected to the same impulsive load.

TABLE 1

THICKNESS MEASUREMENTS OF SPHERE-NOZZLE INTERSECTIONS

See figure 5 for coordinate - grid system.

Thickness measurements given in inches.

a. 6061-T6 Aluminum Specimen No. 1

	A	B	C	E	F	G
1	.1101	.1105	.1107	.0801	.0802	.0806
2	.1100	.1106	.1106	.0803	.0802	.0804
3	.1099	.1104	.1106	.0802	.0804	.0803
4	.1098	.1103	.1105	.0804	.0803	.0805
5	.1099	.1104	.1106	.0803	.0805	.0806
6	.1101	.1106	.1108	.0805	.0806	.0809
7	.1102	.1106	.1109	.0806	.0808	.0810
8	.1104	.1107	.1108	.0809	.0804	.0809

AVERAGE H_s = 0.1104

AVERAGE H_n = 0.0805

VARIATION of H_s = $\pm$ 0.0006

VARIATION of H_n = $\pm$ 0.0005

TABLE 1 (Continued)

b. 6061-T6 Aluminum Specimen No. 2

	A	B	C	E	F	G
1	.1102	.1105	.1108	.0803	.0801	.0804
2	.1104	.1106	.1109	.0806	.0804	.0806
3	.1106	.1108	.1111	.0804	.0807	.0806
4	.1103	.1108	.1111	.0802	.0805	.0803
5	.1107	.1107	.1112	.0800	.0809	.0804
6	.1105	.1108	.1110	.0801	.0810	.0803
7	.1105	.1109	.1113	.0803	.0808	.0802
8	.1106	.1110	.1115	.0802	.0806	.0802

AVERAGE H_s = 0.1108

AVERAGE H_n = 0.0804

VARIATION of H_s = ± 0.0007

VARIATION of H_n = ± 0.0006

TABLE 1 (Continued)

c. 6061-T6 Aluminum Specimen No. 3

	A	B	C	E	F	G
1	.1101	.1104	.1110	.0804	.0806	.0809
2	.1103	.1106	.1110	.0803	.0802	.0810
3	.1100	.1105	.1112	.0809	.0807	.0809
4	.1104	.1107	.1111	.0810	.0809	.0807
5	.1101	.1103	.1113	.0811	.0806	.0802
6	.1102	.1104	.1112	.0810	.0804	.0801
7	.1102	.1105	.1109	.0809	.0801	.0806
8	.1103	.1106	.1108	.0806	.0800	.0804

AVERAGE H_s = 0.1106

AVERAGE H_n = 0.0806

VARIATION of H_s = ± 0.0006

VARIATION of H_n = ± 0.0005

d. 6061-T6 Aluminum Specimen No. 4

	A	B	C	E	F	G
1	.1102	.1108	.1112	.0801	.0806	.0810
2	.1103	.1108	.1113	.0803	.0806	.0811
3	.1101	.1109	.1113	.0806	.0809	.0809
4	.1105	.1107	.1111	.0802	.0810	.0803
5	.1104	.1110	.1114	.0809	.0803	.0807
6	.1107	.1111	.1113	.0805	.0805	.0804
7	.1106	.1109	.1110	.0807	.0802	.0806

AVERAGE H_s = 0.1109

AVERAGE H_n = 0.0806

VARIATION of H_s = ± 0.0006

VARIATION of H_n = ± 0.0005

TABLE 1 (Continued)

e. 6061-T6 Aluminum Specimen No. 5

	A	B	C	E	F	G
1	.1106	.1109	.1111	.0809	.0806	.0807
2	.1107	.1110	.1111	.0805	.0808	.0805
3	.1107	.1113	.1112	.0804	.0803	.0807
4	.1105	.1111	.1114	.0802	.0806	.0809
5	.1108	.1110	.1113	.0806	.0803	.0808
6	.1107	.1109	.1110	.0805	.0804	.0804
7	.1105	.1109	.1112	.0806	.0807	.0809
8	.1104	.1110	.1114	.0808	.0805	.0807

AVERAGE H_s = 0.1109

AVERAGE H_n = 0.0806

VARIATION of H_s = $\pm$0.0005

VARIATION of H_n = $\pm$0.0004

TABLE 2

OFFSETS FOR DETERMINING OUTSIDE DIAMETER OF SPHERE

See Figure 7 for coordinate system

Coordinates given in inches.

a. 6061-T6 Aluminum Specimen No. 1

POINT	X	Y
0	0	0
1	0.500	0.1305
2	0.750	0.2380
3	1.000	0.3795
4	1.250	0.5625
5	1.500	0.8005
6	1.750	1.1245

TABLE 2 (Continued)

b. 6061-T6 Aluminum Specimen No. 2

POINT	X	Y
0	0	0
1	0.250	0.0435
2	0.500	0.1040
3	0.750	0.1900
4	1.000	0.3070
5	1.250	0.4600
6	1.500	0.6595
7	1.750	0.9330
8	2.000	1.3460

TABLE 2 (Continued)

c. 6061-T6 Aluminum Specimen No. 3 .

POINT	X	Y
0	0	0
1	0.250	0.0500
2	0.500	0.1215
3	0.750	0.2210
4	1.000	0.3525
5	1.250	0.5230
6	1.500	0.7525
7	1.750	1.0745
8	1.875	1.3020

TABLE 2 (Continued)

d. 6061-T6 Aluminum Specimen No. 4

POINT	X	Y
0	0	0
1	0.250	0.0500
2	0.500	0.1205
3	0.750	0.2280
4	1.000	0.3570
5	1.250	0.5230
6	1.500	0.7450
7	1.750	1.0565
8	1.875	1.3010

TABLE 2 (Continued)

e. 6061-T6 Aluminum Specimen No. 5

POINT	X	Y
0	0	0
1	0.250	0.0520
2	0.500	0.1280
3	0.750	0.2315
4	1.000	0.3690
5	1.250	0.5480
6	1.500	0.7825
7	1.750	1.1035
8	1.875	1.2320

TABLE 3

DATA FOR 6061-T6 ALUMINUM SPHERE-CYLINDRICAL NOZZLE INTERSECTIONS

SPHERE

Spec. No.	D_s in	H_s in	M_s $10^{-4}\frac{lb\text{-}sec^2}{in}$	W_{es} gm	I_s lb-sec
1	4.95	0.1104	9.89	5.45	2.227
2	4.91	0.1108	9.84	4.68*	1.897
3	4.82	0.1106	9.63	3.98*	1.642
4	4.75	0.1109	9.49	3.80*	1.568
5	5.11	0.1109	10.25	8.08	3.333

NOZZLE

Spec. No.	D_n in	H_n in	L in	M_n $10^{-4}\frac{lb\text{-}sec^2}{in}$	W_{en} gm	I_n lb-sec
1	2.039	0.0805	4.025	5.11	0.00	0.000
2	2.056	0.0804	4.007	5.16	3.89*	1.604
3	2.039	0.0806	4.023	5.12	4.45*	1.835
4	2.040	0.0806	3.946	5.12	2.81*	1.159
5	2.040	0.0806	4.161	5.12	6.71	2.767

*Denotes that explosive was perforated to reduce the total impulse.

TABLE 3 (Continued)

SPHERE

Spec. No.	W* in	W^*/H_s	λ_s	V_s in/sec
1	.0322	0.292	62.3	2252
2	.0546	0.520	44.6	1927
3	.0310	0.280	32.5	1705
4	.0278	0.251	30.3	1652
5	-	-	134.3	3217

NOZZLE

Spec. No.	W* in	W^*/H_n	λ_n	V_n
1	.0248	.308	000	0000
2	.0498	.620	39.0	3110
3	.0514	.636	50.5	3583
4	.0365	.452	20.1	2263
5	-	-	114.8	5403

TABLE 4

PERMANENT DEFLECTION DATA FOR SPHERE-CYLINDRICAL

NOZZLE INTERSECTIONS

Deflections are in inches. See Figure 5 for coordinate-grid system.

a. Specimen No. 1

	A	B	C	D	E	F	G
1	.0039	.0455	.0264	.0122	.007	.011	.025
2	.0167	.0598	.0335	.0118	.001	.009	.024
3	.0329	.0767	.0287	.0112	.007	.008	.032
4	.0386	.0770	.0357	.0109	.011	.013	.031
5	.0435	.0607	.0371	.0121	.007	.008	.024
6	.0385	.0708	.0363	.0116	.004	.004	.017
7	.0114	.0619	.0334	.0116	.006	.005	.020
8	-.0125	.0456	.0264	.0124	.009	.007	.025

Positive direction is radially outward.

TABLE 4 (Continued)

b. Specimen No. 2

	A	B	C	D	E	F	G
1	.0365	.0698	.0620	-.0461	.042	.128	.037
2	.0298	.0452	.0648	-.0399	.030	.078	.028
3	.0072	.0386	.0605	-.0472	.025	.102	.042
4	.0163	.0577	.0708	-.0446	.047	.128	.068
5	.0259	.0306	.0534	-.0608	.037	.122	.064
6	.0125	.0051	.0336	-.0519	.007	.080	.058
7	-.0082	.0129	.0380	-.0419	.005	.090	.064
8	.0217	.0633	.0610	-.0464	.044	.129	.038

TABLE 4 (Continued)

c. Specimen No. 3

	A	B	C	D	E	F	G
1	.0006	.0106	.0192	-.0792	.022	.136	.035
2	.0104	.0001	.0191	-.0627	.037	.111	.087
3	.0075	.0052	.0304	-.0652	.096	.127	.084
4	-.0022	-.0044	.0216	-.0747	.112	.165	.061
5	.0125	.0088	.0141	-.0538	.025	.149	.032
6	.0309	.0523	.0514	-.0618	.027	.104	.035
7	.0314	.0501	.0510	-.0832	.067	.144	.044
8	.0116	.0315	.0414	-.0884	.065	.167	.037

TABLE 4 (Continued)

d. Specimen No. 4

	A	B	C	D	E	F	G
1	.0107	.0325	.0333	-.0123	.023	.062	.054
2	.0175	.0263	.0344	-.0106	.011	.056	.038
3	.0189	.0053	.0225	-.0103	.004	.028	.020
4	.0034	.0046	.0225	-.0162	.031	.033	.040
5	.0053	.0237	.0458	-.0117	.018	.046	.061
6	.0135	.0216	.0258	-.0201	.010	.033	.034
7	.0113	-.0005	.0149	-.0177	-.007	.022	.011
8	.0116	.0155	.0233	-.0162	.014	.022	.034

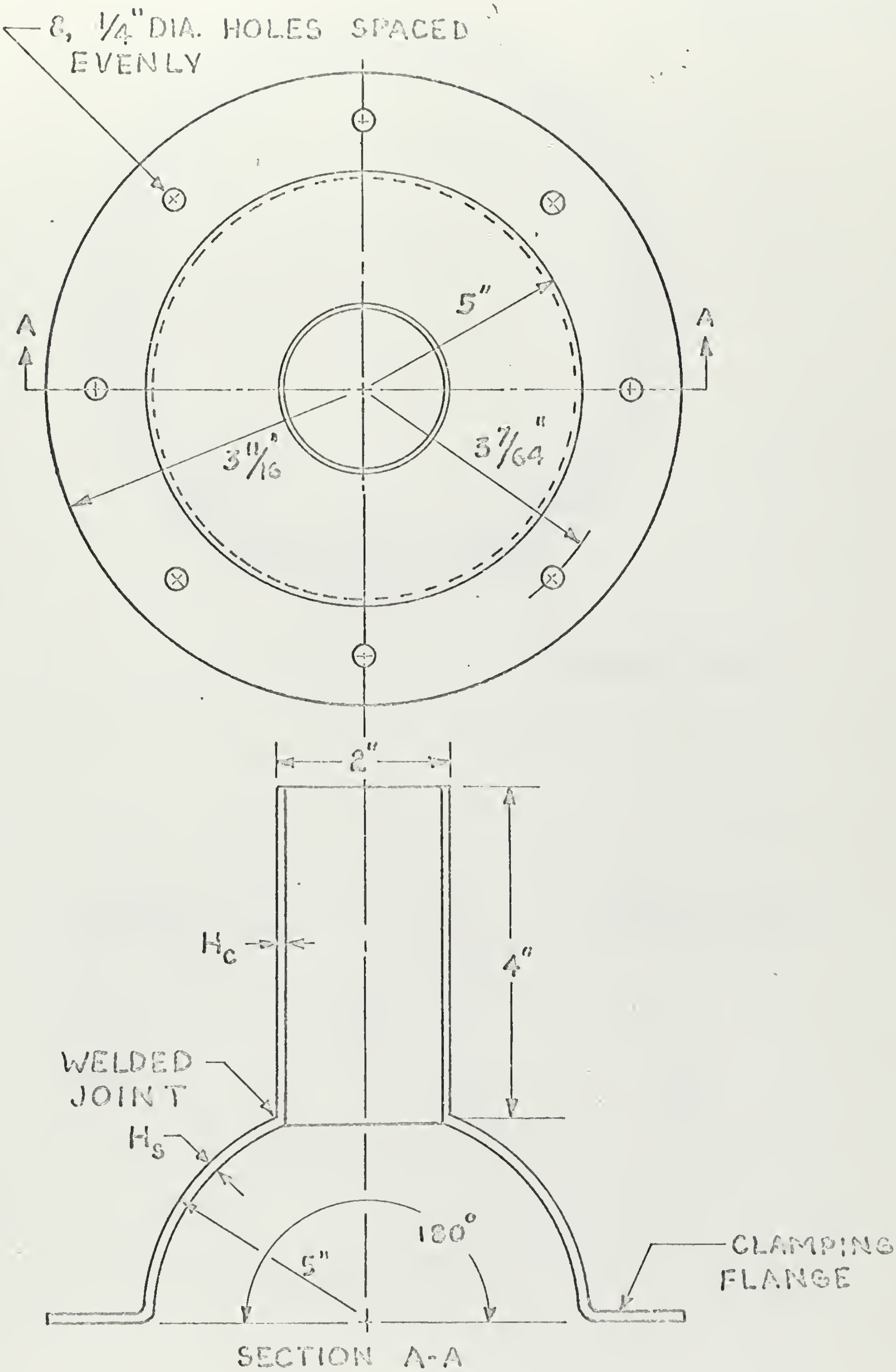

8, 1/4" DIA. HOLES SPACED EVENLY
A
A
5"
3 11/16"
3 7/64"
2"
4"
H_c
WELDED JOINT
H_s
180°
5"
CLAMPING FLANGE
SECTION A-A

FIGURE 1

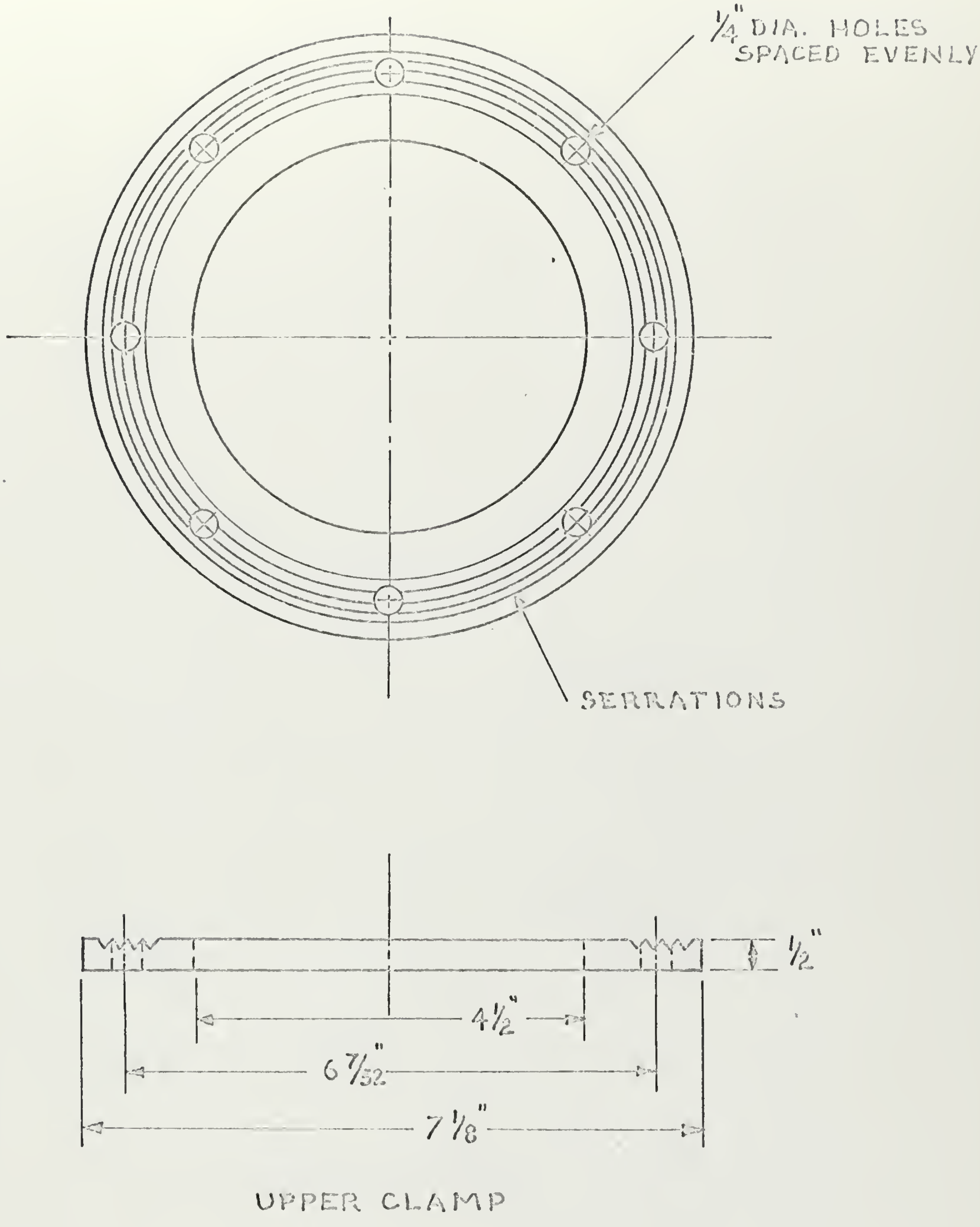

1/4" DIA. HOLES
SPACED EVENLY
SERRATIONS
1/2"
4 1/2"
6 7/32"
7 1/8"
UPPER CLAMP

FIGURE 2a

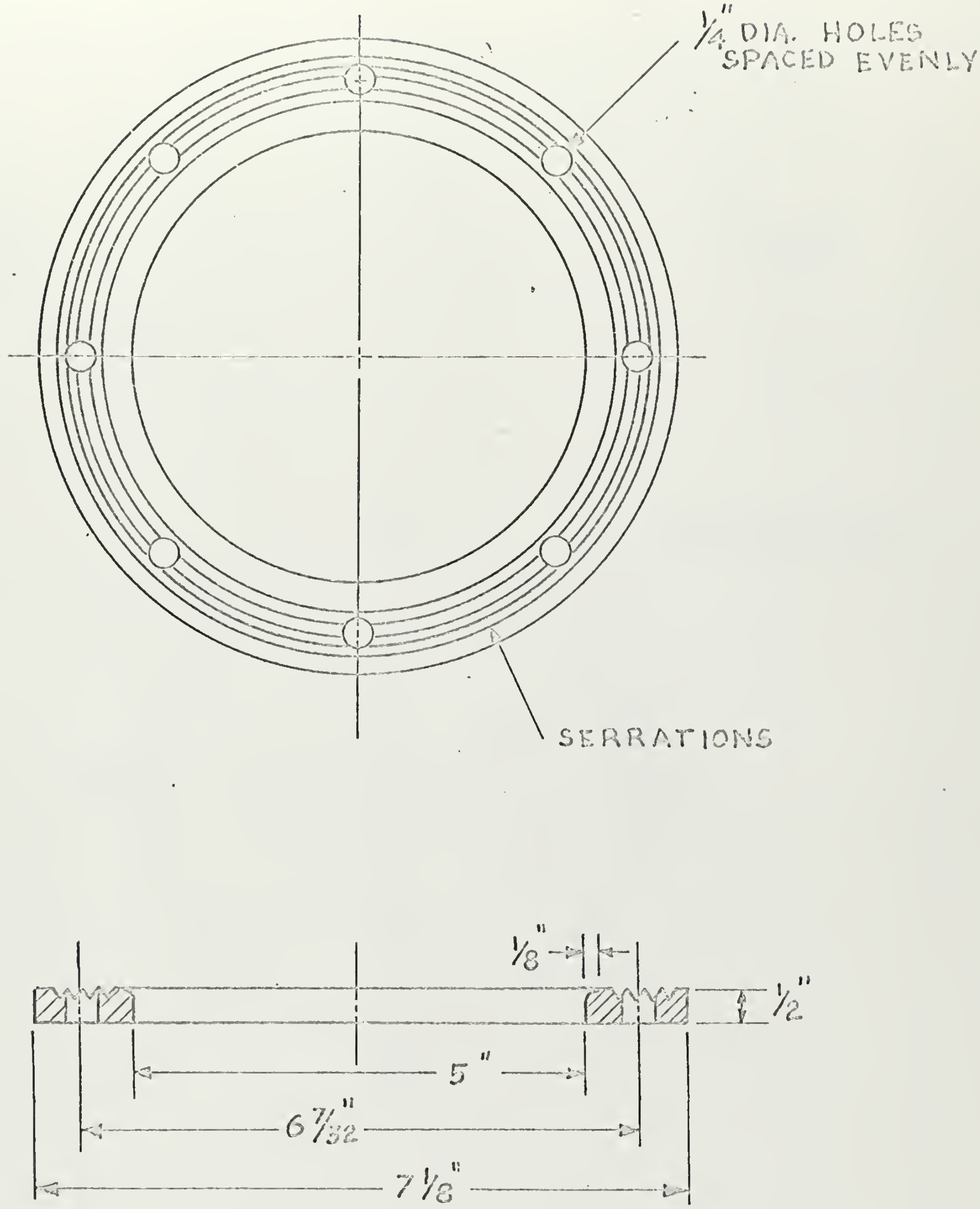

LOWER CLAMP

FIGURE 2b

TABLE ADAPTER PLATE 1/2" THICK

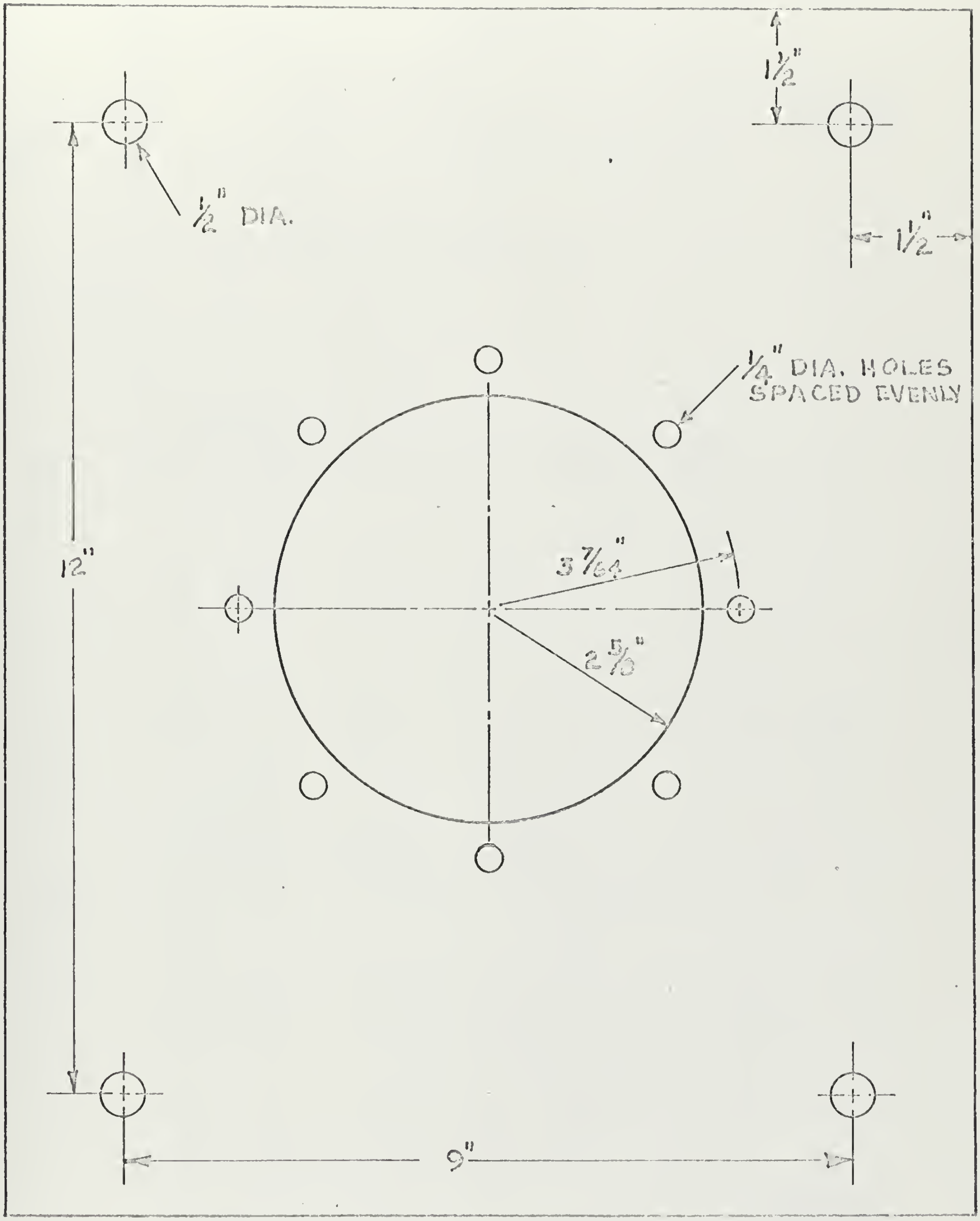

FIGURE 2c

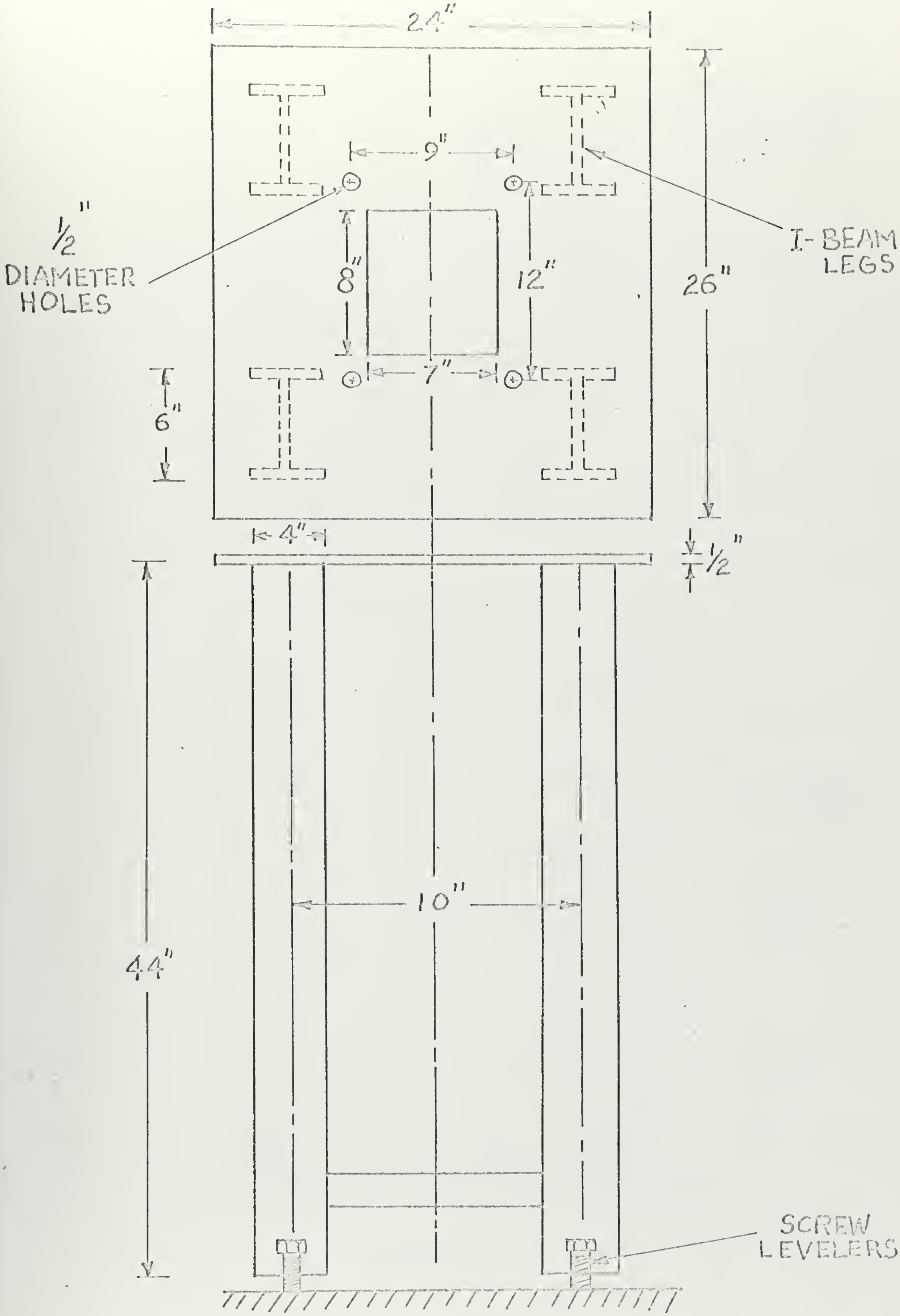
24"
9"
1/2" DIAMETER HOLES
I-BEAM LEGS
8"
12"
26"
7"
6"
4"
1/2"
10"
44"
SCREW LEVELERS

FIGURE 3

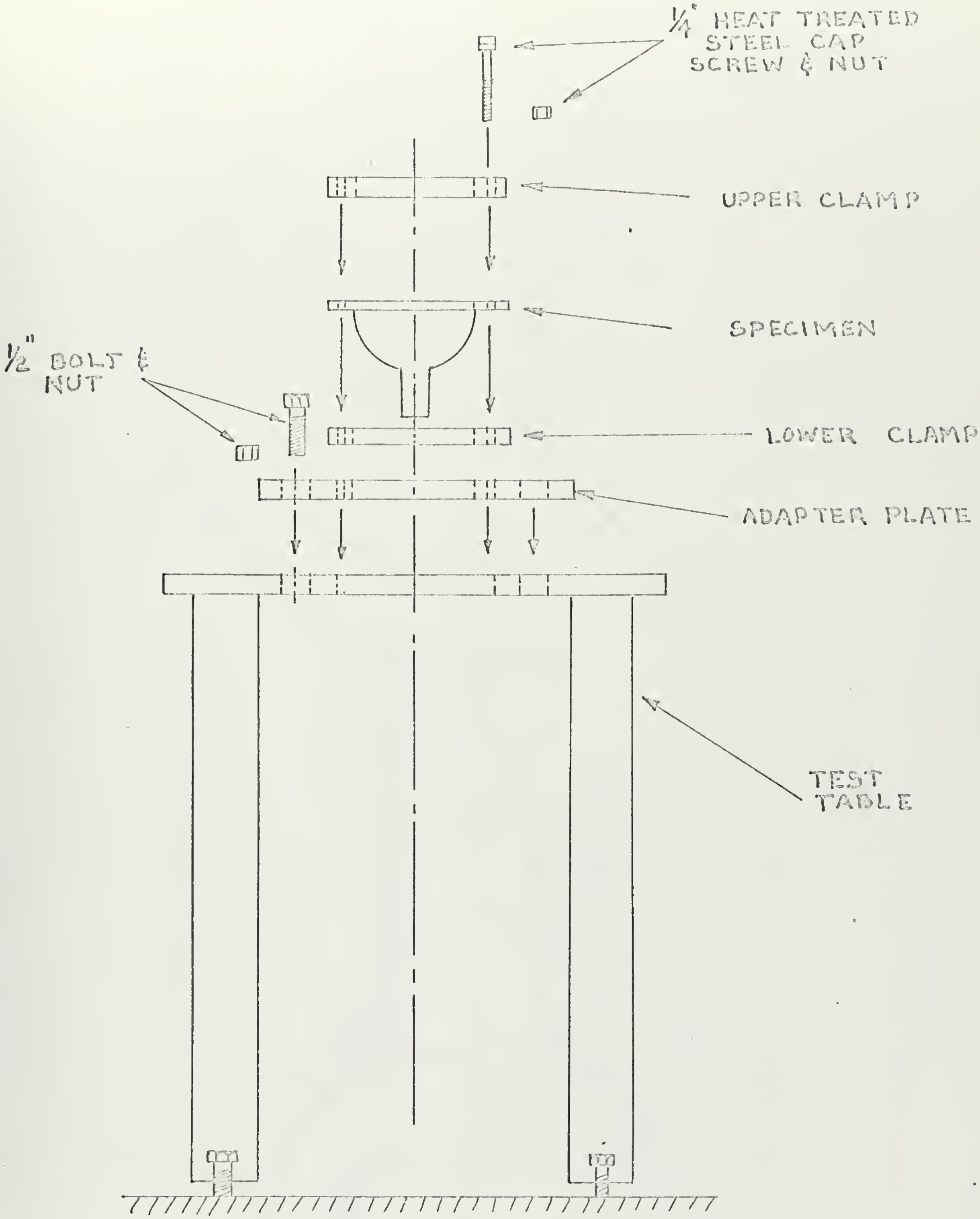

1/4" HEAT TREATED STEEL CAP SCREW & NUT
UPPER CLAMP
SPECIMEN
1/2" BOLT & NUT
LOWER CLAMP
ADAPTER PLATE
TEST TABLE

FIGURE 4

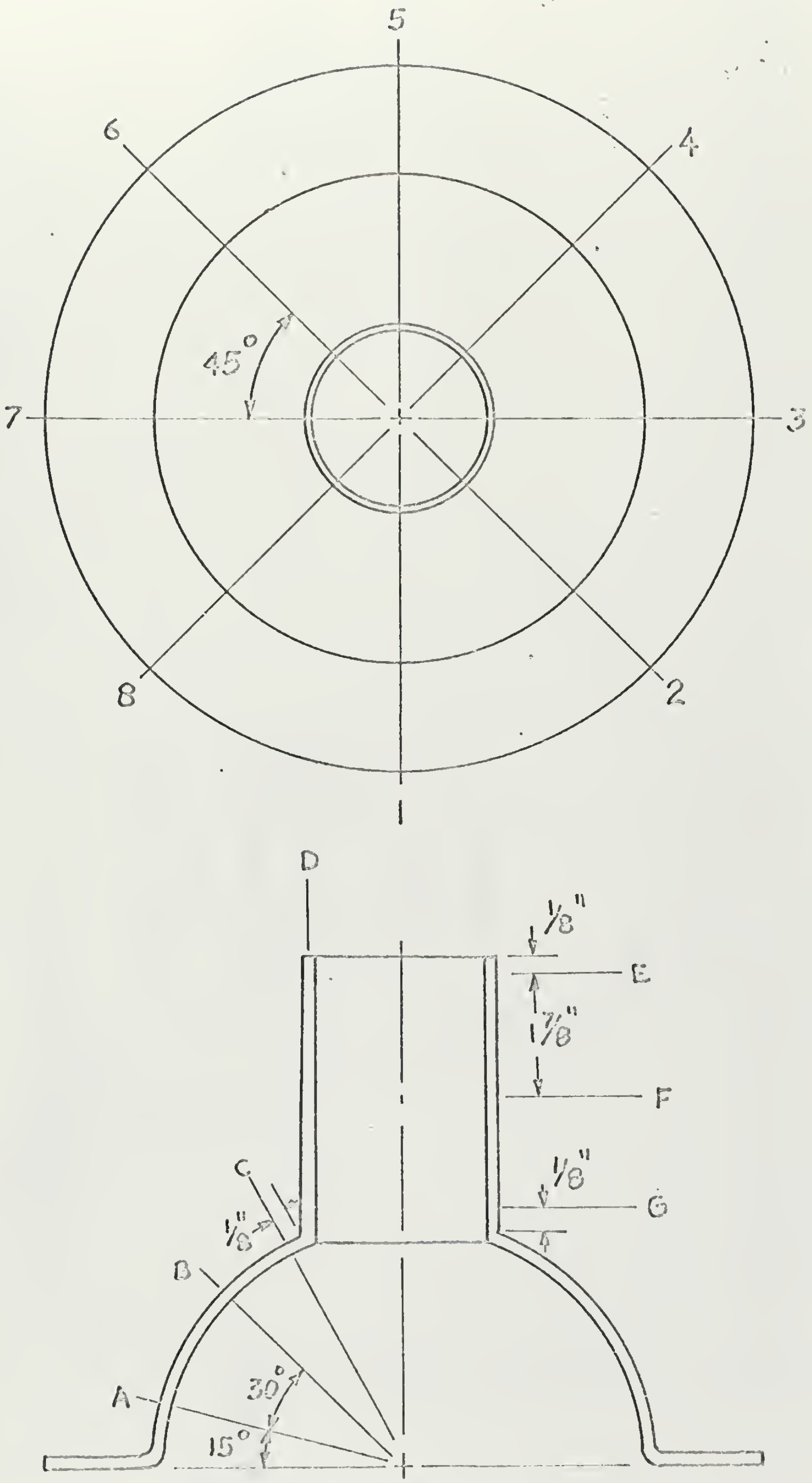

COORDINATE - GRID SYSTEM

FIGURE 5

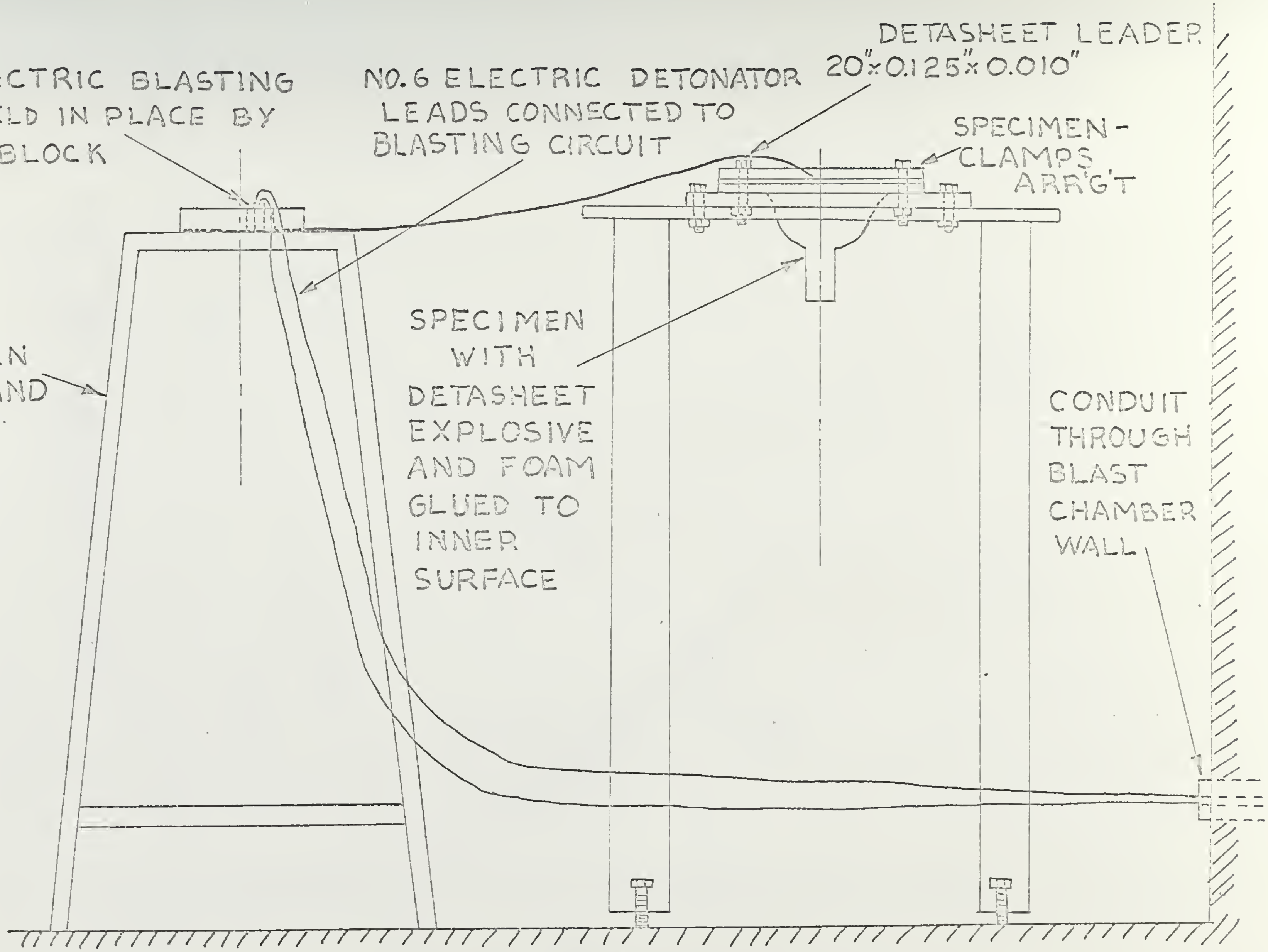
DETASHEET LEADER
20"x0.125"x0.010"
NO.6 ELECTRIC BLASTING
CAP HELD IN PLACE BY
STEEL BLOCK
NO.6 ELECTRIC DETONATOR
LEADS CONNECTED TO
BLASTING CIRCUIT
SPECIMEN-
CLAMPS
ARR'G'T
WOODEN
STAND
SPECIMEN
WITH
DETASHEET
EXPLOSIVE
AND FOAM
GLUED TO
INNER
SURFACE
CONDUIT
THROUGH
BLAST
CHAMBER
WALL

FIGURE 6

SPECIMEN No. 4
SCALE: 1" = 0.5"

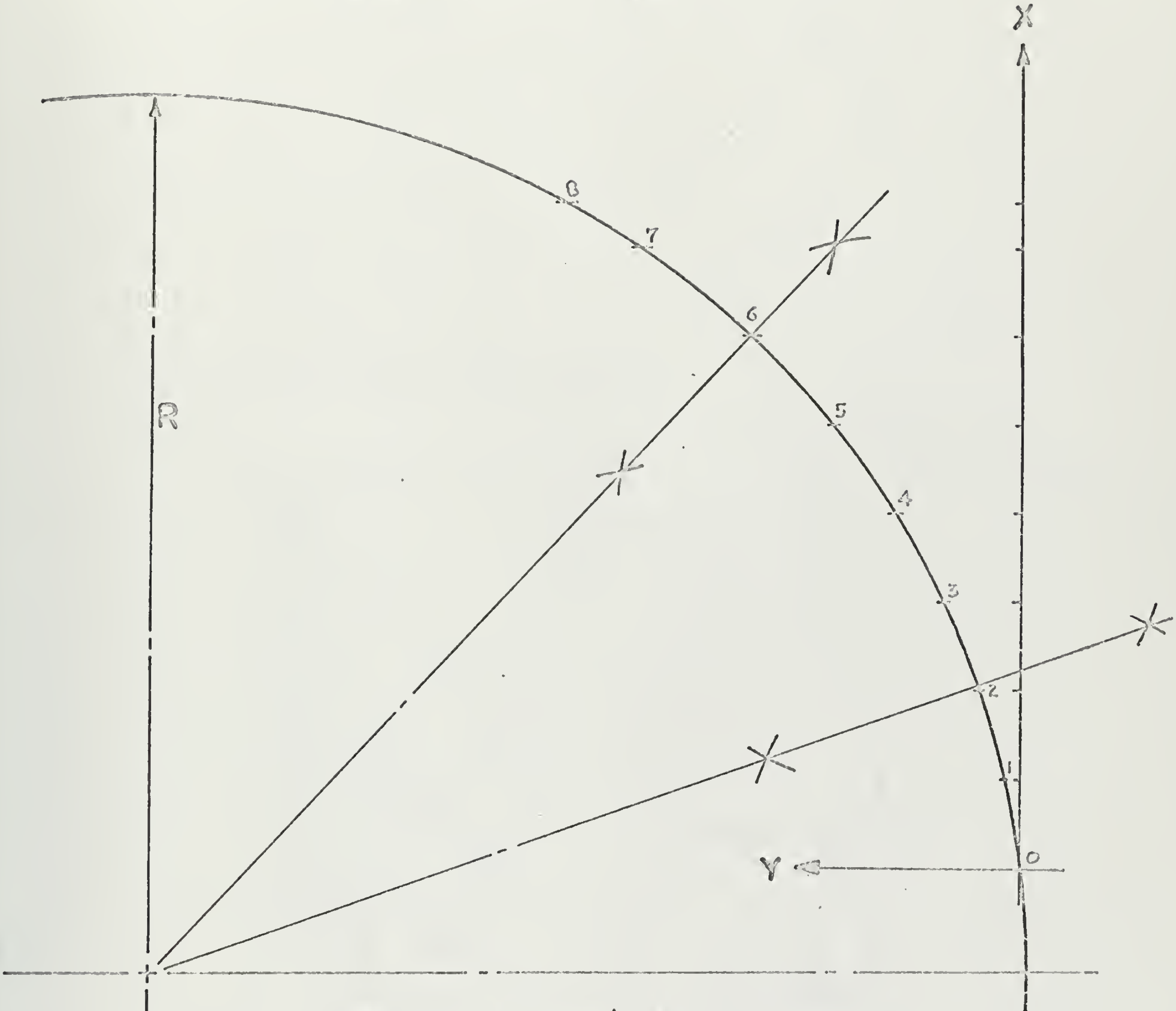

COORDINATE SYSTEM & TYPICAL PLOT FOR DETERMINING SPHERE OUTSIDE DIAMETER

FIGURE 7

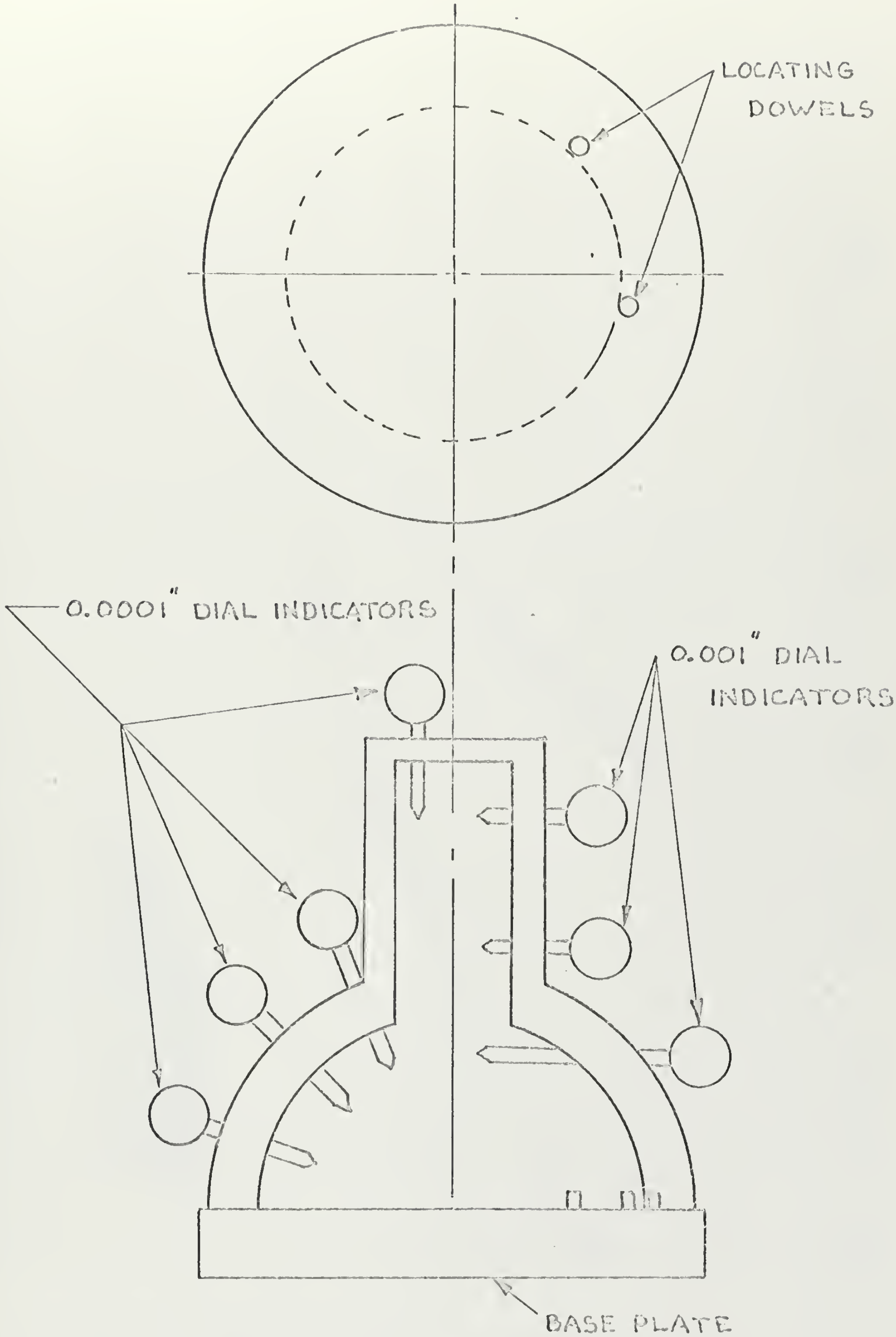

MEASURING APPARATUS

FIGURE 8

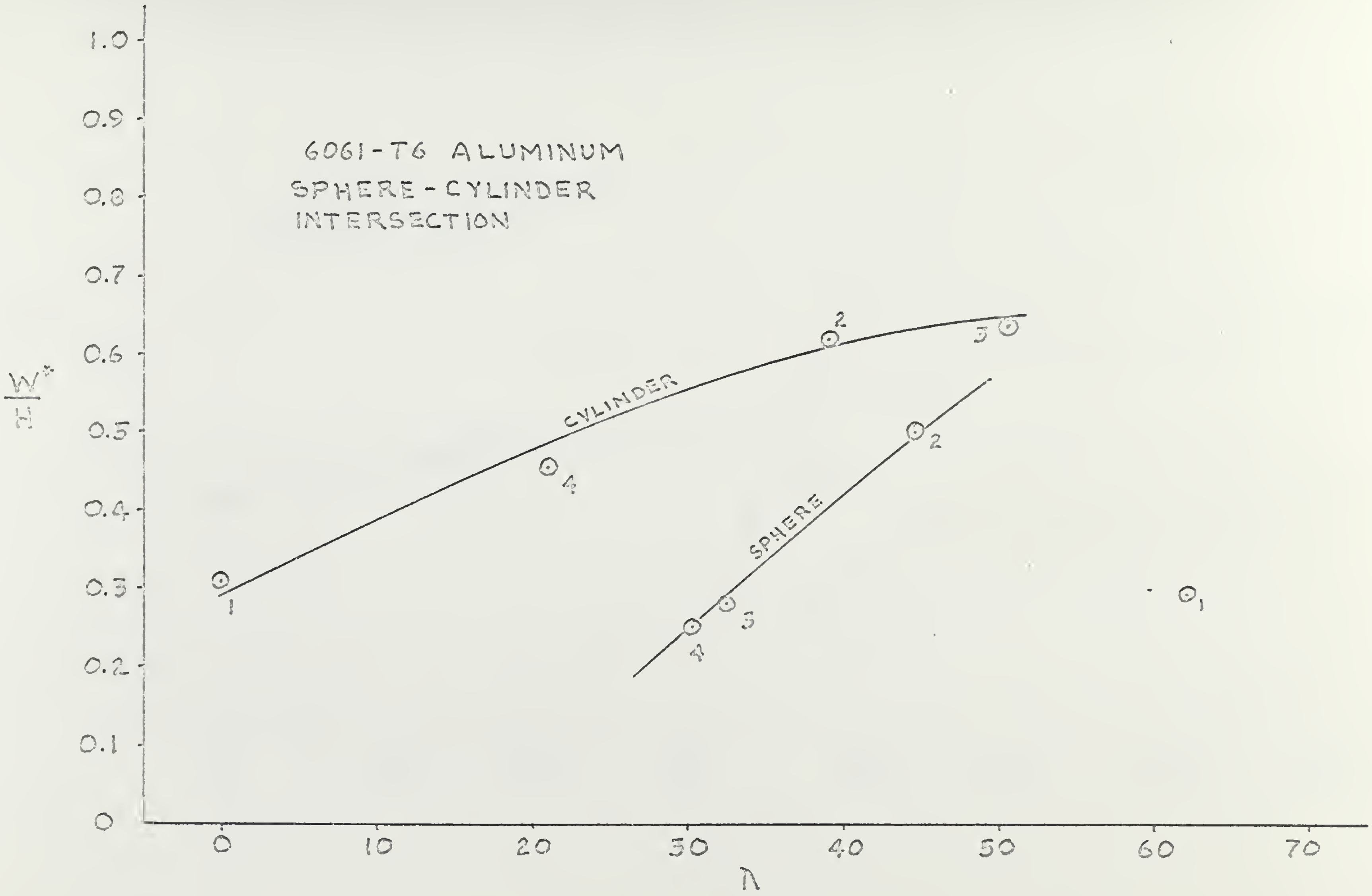
6061-T6 ALUMINUM
SPHERE-CYLINDER
INTERSECTION
$\frac{W^*}{H}$
1.0
0.9
0.8
0.7
0.6
0.5
0.4
0.3
0.2
0.1
0
CYLINDER
SPHERE
1
2
3
4
5
0
10
20
30
40
50
60
70
λ

FIGURE 9

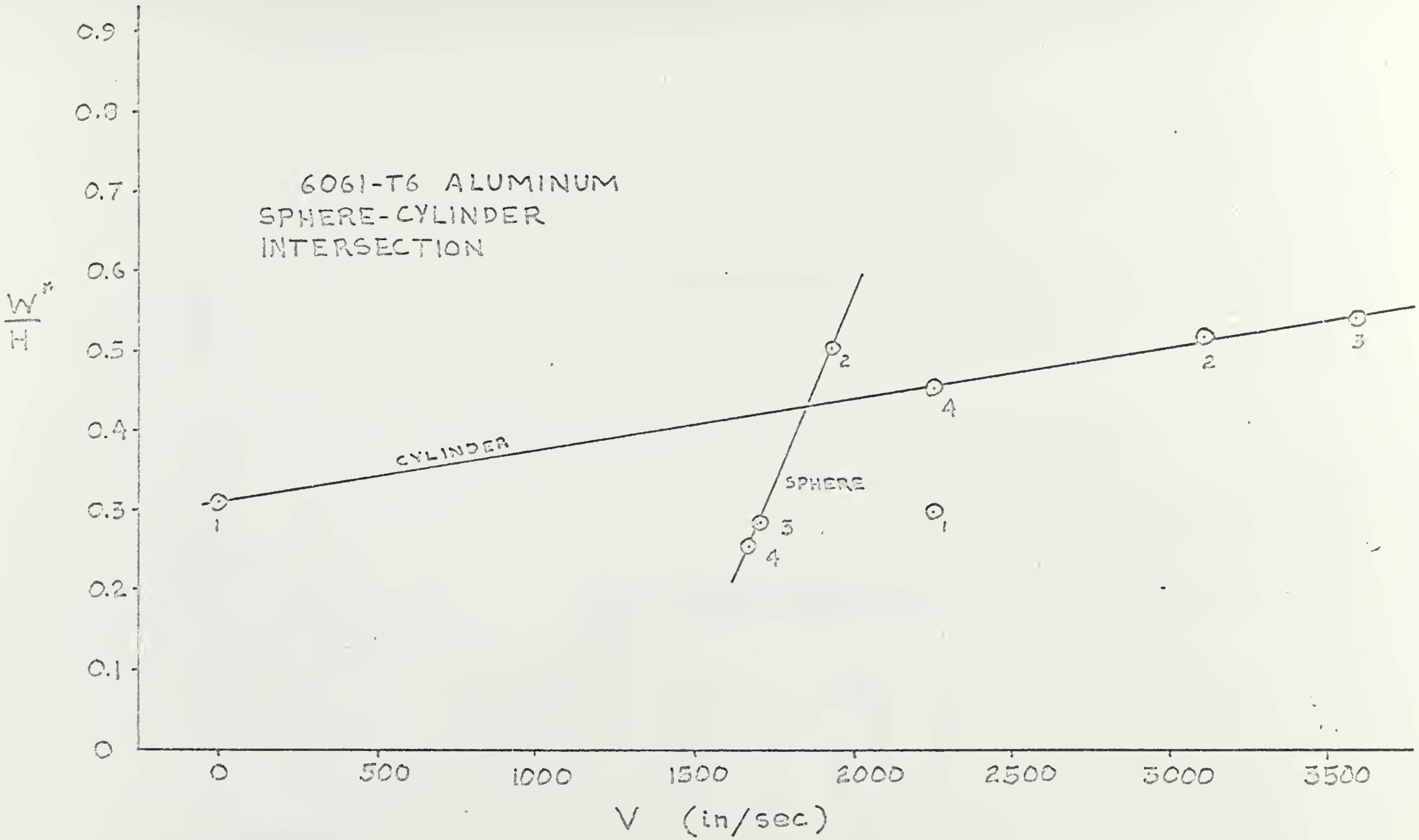
6061-T6 ALUMINUM
SPHERE-CYLINDER
INTERSECTION
W"/H
0.9
0.8
0.7
0.6
0.5
0.4
0.3
0.2
0.1
0
CYLINDER
SPHERE
0
500
1000
1500
2000
2500
3000
3500
V (in/sec)

FIGURE 10

SPECIMEN NO. 1
AVERAGE DEFLECTIONS PLOTTED

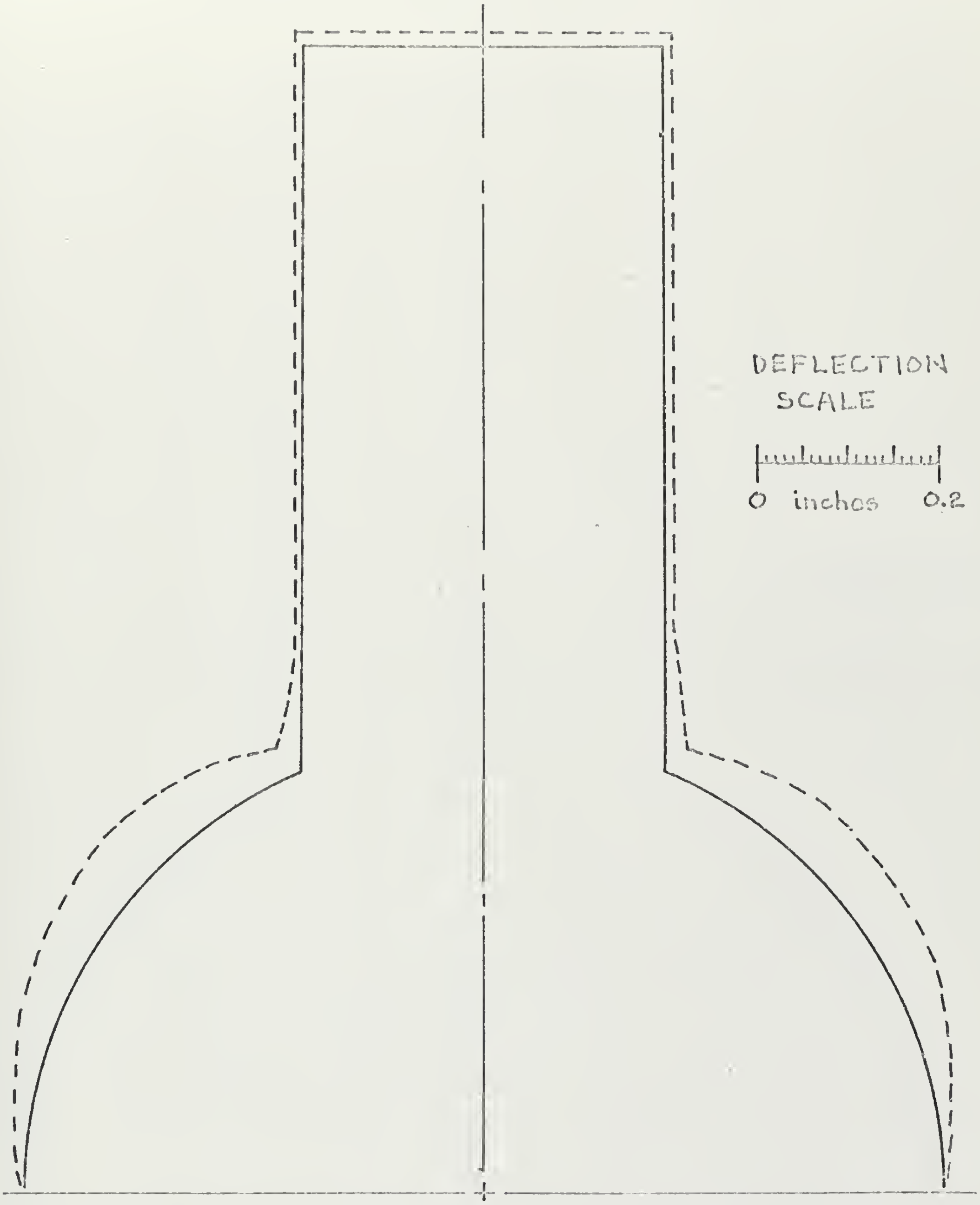

DEFORMATION PROFILE

FIGURE 11-a

SPECIMEN NO. 2

AVERAGE DEFLECTIONS PLOTTED

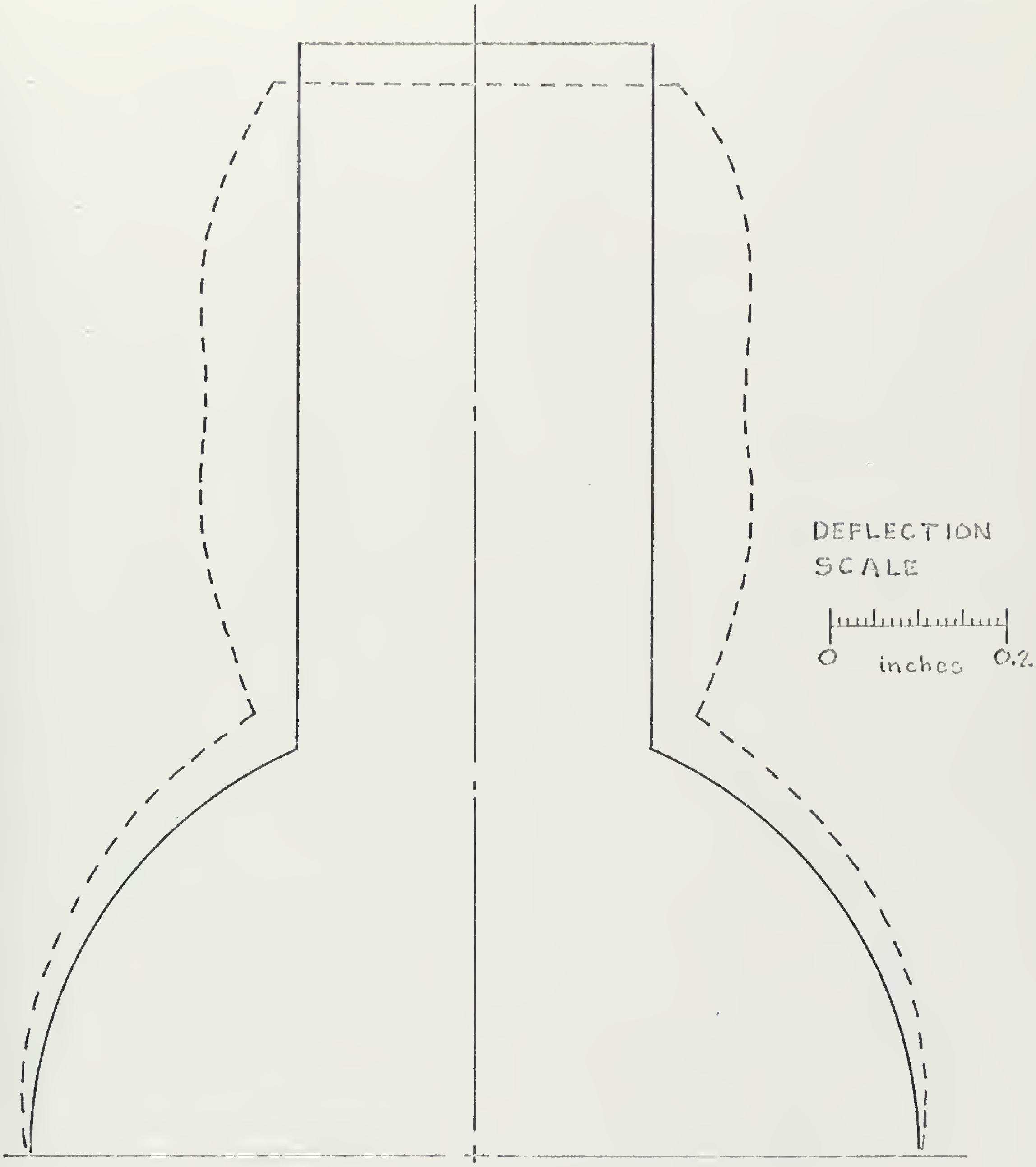

DEFORMATION PROFILE

FIGURE II-6

SPECIMEN NO. 3
AVERAGE DEFLECTIONS PLOTTED

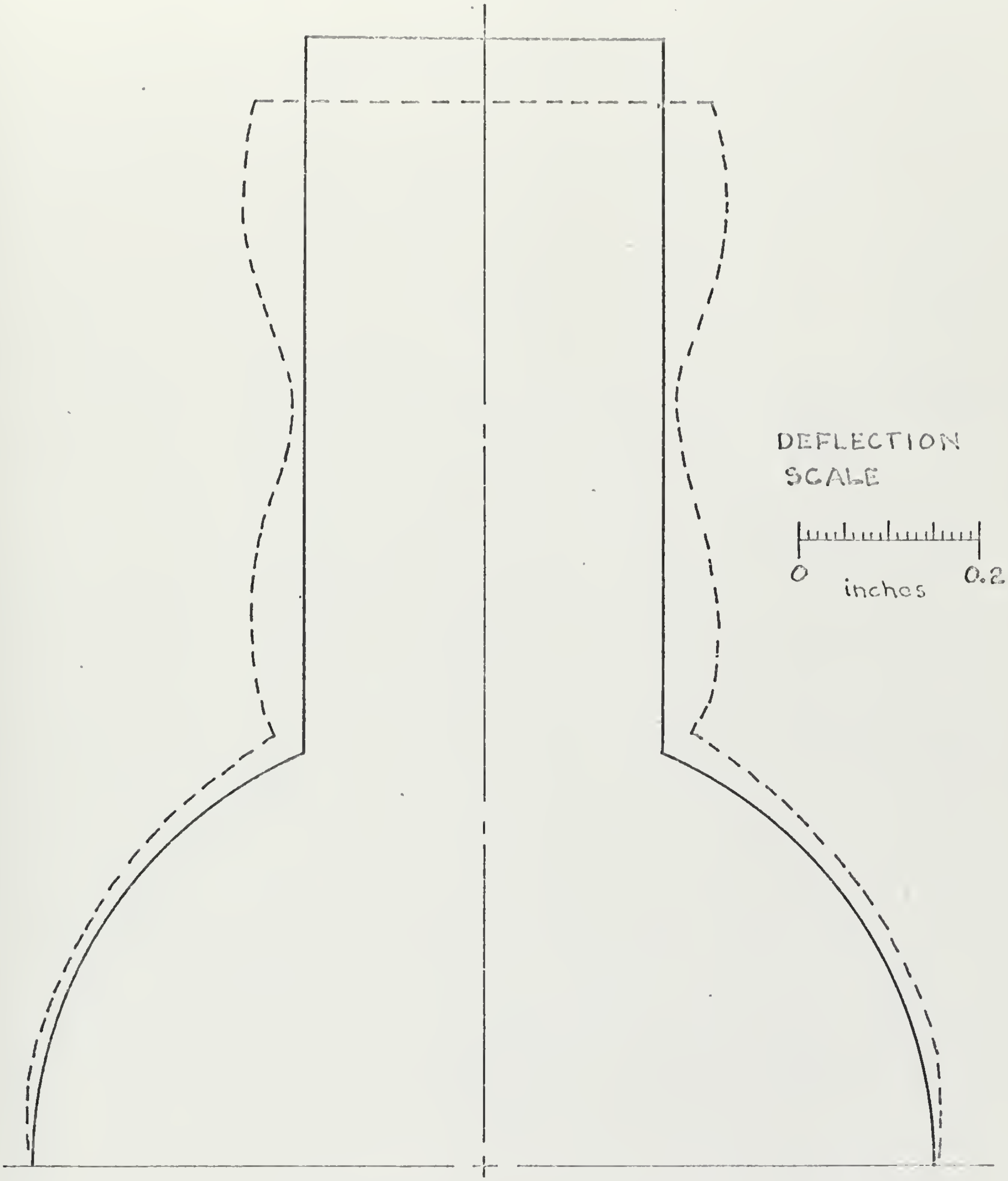

DEFORMATION PROFILE

FIGURE II-c

SPECIMEN NO. 4

AVERAGE DEFLECTIONS PLOTTED

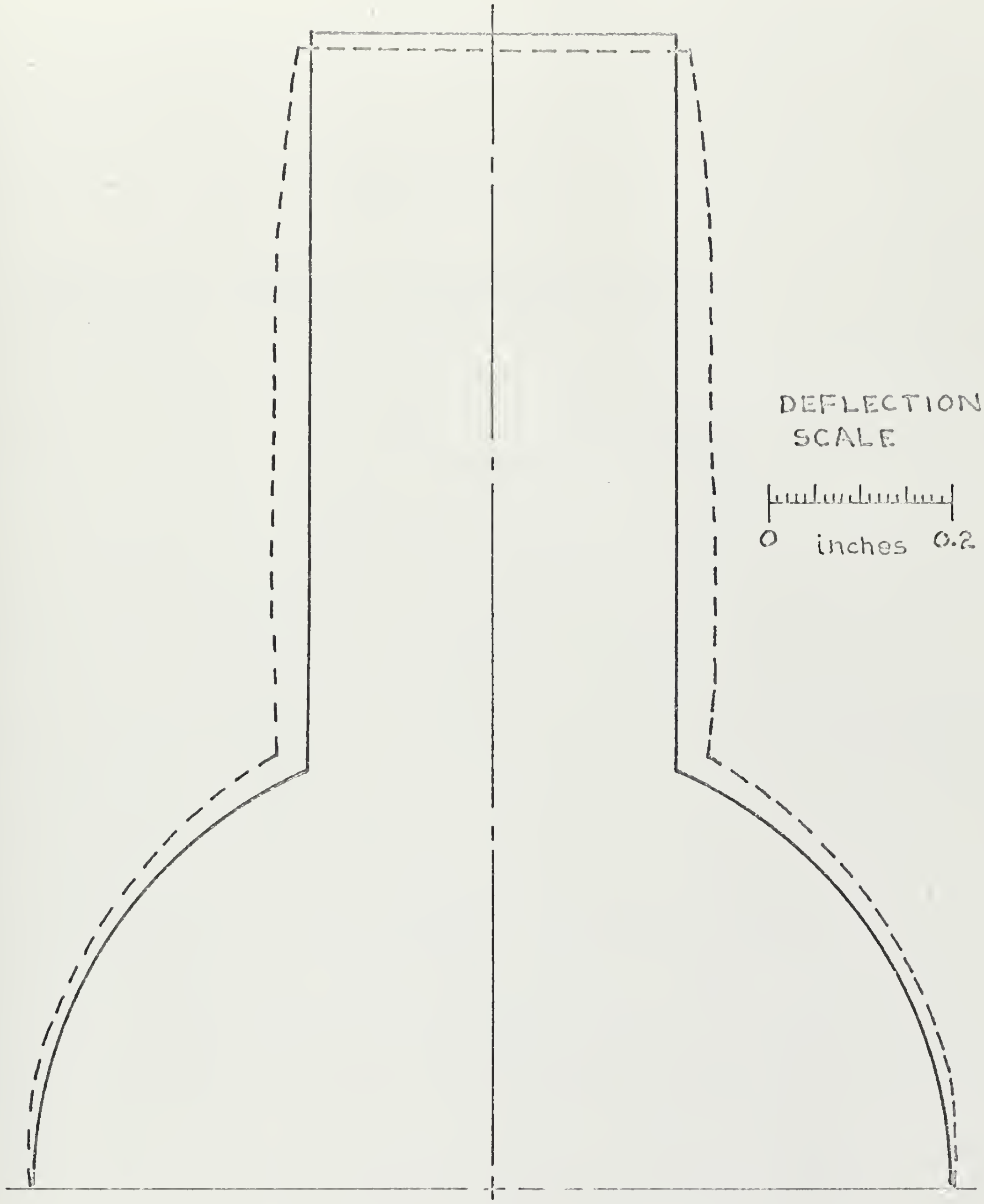

DEFORMATION PROFILE

FIGURE 11-d

SECTION II

TESTS ON 90 DEGREE CYLINDRICAL PANELS

NOMENCLATURE

H_e	thickness of sheet explosive
H_s	thickness of specimen
I	total impulse $I = I_o W_e$
I_o	specific impulse
L	semi-length of cylindrical panel
L_e	length of explosive
D	mean diameter of cylindrical panel
R	mean radius of cylindrical panel
M_s	mass of specimen acted on by initial velocity V_o
V_o	initial velocity of specimen
W_e	weight of explosive
δ	radial deflection of specimen
δ_m	maximum permanent radial deflection of specimen
δ_o	permanent radial deflection at center of specimen
η	impulse parameter
ρ	mass density
σ_o	yield stress of material in simple tension
SE	strain energy $SE = \frac{\sigma_o^2}{2E}$ (Vol)
KE	initial kinetic energy $KE = \frac{1}{2} M_s V_o^2$
ER	energy ratio $ER = KE/SE$
Vol	total volume of panel between clamped edges

EXPERIMENTAL PROCEDURE

In addition to tests conducted on the intersecting shells, a series of tests were also conducted on 90 degree cylindrical panels.

The test specimens and experimental procedure used were primarily the same as those used by Dumas (6). Six tests were conducted on hot-rolled mild steel panels with a nominal thickness of 0.108 inches and six tests were conducted on 6061-T6 aluminum panels with a nominal thickness of 0.091 inches. The procedure and apparatus for measuring deflections was the same as used by Dumas.

Each specimen was loaded with a 2in x 3in rectangular sheet of DuPont "Detasheet" explosive placed on the geometric center of the specimen's inner surface. A 1/4 inch thick foam attenuator was used between the specimen and the explosive. This is the same explosive-attenuator system used by Dumas.

A re-calculation of the calibration tests conducted by Dumas was done. This resulted in a different specific impulse, I_o, than that reported by Dumas. The actual specific impulse was found to be 19.20 x 10^4 dyne-sec/gm or 0.430 lb-sec/gm. Some of the tests were conducted using a different batch of explosive than that used by Dumas. This new explosive was found to have a specific impulse of 18.42 x 10^4 dyne-sec/gm or 0.4125 lb-sec/gm. (See Appendix B)

It became apparent during the calculation for the intial velocity, V_o, that the values reported by Dumas were incorrect, not only from the use of a lower value for the specific impulse, I_o, but also from the calculation of the specimen mass, M_s, and the determination of the mean diameter, D.

The correct definition of the specimen mass is the mass of the specimen over which the initial velocity acts as shown in figure (II-1).

From figure (II-1), it can be seen that, M_s, is not the same as the mass of the entire specimen between the clamped edges.

In the determination of M_s, it is necessary to calculate the mean arc length over which the initial velocity acts. From figure (II-2), it can be seen that the mean radius, R, is:

$$R = r_e + (H/2 + T) \qquad (1)$$

Where T is the thickness of the foam attenuator (1/4 inch for the tests conducted here). The arc length of the explosive is:

$$S_e = r_e\phi \qquad (2)$$

And that the mean arc length, S, is:

$$S = R\phi \qquad (3)$$

Or

$$S = S_e \left[\frac{R}{R - (H/2 + T)}\right] \qquad (4)$$

Using

$$D = 2R \text{ and } T = 1/4 \text{ inch} \tag{5}$$

And

$$B = 2(H/2 + 1/4) \tag{6}$$

The mean arc length becomes:

$$S = S_e \left[\frac{1}{1 - B/D} \right] \tag{7}$$

The mass of the specimen now becomes:

$$M_s = \rho S H_s L_e \tag{8}$$

Since we have that:

$$V_o = \frac{I_o W_e}{M_s} \tag{9}$$

We have

$$V_o = \frac{I_o W_e (2D - 2H_s - 1)}{2 \rho H_s D L_e S_e} \tag{10}$$

We now define λ as:

$$\lambda = \frac{V_o^2 D^2}{4 \sigma_o H_s^2} \tag{11}$$

Which gives

$$\lambda = \frac{I_o^2 W_e^2 (2D - 2H_s - 1)^2}{16 \rho \sigma_o L_e^2 S_e^2 H_s^4} \tag{12}$$

From equation (12), it appeared that there was a major step in the experimental procedure that might be different from the procedure previously used by Dumas. This was in the measurement of the mean specimen diameter. In the additional specimens tested, the mean diameter was measured by tracing the outline of the specimen and measuring the outside diameter, D_o, of each specimen and

the mean diameter found by using:

$$D = D_o - H_s \tag{13}$$

The hydroforming process used to make the specimens uses a mold to give the specimen an outside diameter of 4 inches while in the mold.

The results reported by Dumas makes the assumption that the outside diameter of each finished specimen is in fact four inches. This assumption does not account for the elastic strain which relaxes when the specimen is removed from the mold. This relaxation tends to increase the specimen diameter. From examining equation (12), it is seen that both λ and $\lambda(H_s/R)$ are highly sensitive to the mean diameter measurement.

The assumption was made that the included angle between the clamped edges, Θ, as reported by Dumas was correct. The width of the clamp opening was measured and found to be 3.00 inches. By using the following:

$$D_o = \frac{3.00}{\sin(\Theta/2)} \text{ inches} \tag{14}$$

a new outside diameter was calculated. The mean diameter was then calculated by using equation (13).

DISCUSSION OF RESULTS

Tables II-1a and II-1b give the results of using the corrected data for the hot-rolled mild steel specimens. Tables II-2a and II-2b give the results for the 6061-T6 aluminum specimens.

Appendix A give the mechanical properties for each material and specimen thickness. The cross head speed of the tensile test machine was 0.1 in/min for all cases.

Tensile tests were conducted in two directions on the plate perpendicular to each other. An average value of these results was used as the yield strength in calculating results.

A variation of thickness ± 0.0002in was observed in the new hot-rolled mild steel and 6061-T6 aluminum panels tested.

The experimental values of permanent deflections resulting from a uniformly distributed total impulse, I, is presented for mild steel and 6061-T6 aluminum specimens in figures II-3 and II-4 respectively. The maximum deflection occurred at the center of the cylindrical panel in most cases, as expected; therefore the center point deflection, δ_0, was used for consistency in all cases. It is seen that the permanent deflection is a non-linear function of total impulse.

The permanent deflections for each of the additional specimens tested are tabulated in Tables II-3 and II-4.

The deflection parameter δ_0/H_s is plotted as a function of the impulse parameter $\lambda \, H_s/R$ in figure II-6. It is evident from this figure that permanent deflections of panels made from mild steel are smaller than deflections of similar panels made of 6061-T6 aluminum. This is believed to be due to the difference in strain-rate sensitivity of the materials. The mild steel is strain-rate sensitive while the 6061-T6 aluminum is relatively insensitive to strain-rate.

While figure II-6 shows a non-linear relationship, the curves appear linear over a range of δ_0/H_s less than 1.0. Therefore, it is felt that bending only theory might predict results which reasonably approximate the experimental results for a range of δ_0/H_s less than 1.0.

CONCLUSIONS

It is shown that the permanent deflections are non-linear functions of total impulse. By extending the lines plotted, an estimate of the minimum value of impulse that would produce a permanent deflection might be obtained.

It is evident that the permanent deflections for the mild steel specimens are less than those of geometrically similar 6061-T6 aluminum cylindrical panels subjected to the same magnitudes of total impulse. It is concluded that this is due to the different material strain-rate sensitivities of the two materials tested.

It is also concluded that reasonable results might be obtained by neglecting finite deflections for impulsive loading when δ_o/H_s is less than approximately 1.0.

It is recommended that additional tests be conducted for varying panel thicknesses over a wider range of impulse than that examined here. It must be pointed out here that values of δ_o/H_s greater than about 2.0 might be difficult to obtain for 6061-T6 aluminum panels. This material tends to exhibit shear along the clamped edges for impulses greater than those leading to a δ_o/H_s of about 2.0.

TABLE II-1a

DATA FOR HOT-ROLLED MILD STEEL SPECIMENS

Spec. No.	D in	2_L in	H_s in	Θ deg	W_e gm	I_o lb-sec/gm	I lb-sec
1	4.11	5.98	.1206	90.4	4.76	0.430	2.047
2	4.10	5.99	.1206	90.6	6.27	0.430	2.696
3	4.07	5.98	.1202	91.2	3.37	0.430	1.449
4	4.07	5.98	.1209	91.2	5.02	0.430	2.159
5	4.11	5.98	.1205	90.4	5.77	0.430	2.481
6	4.14	5.98	.0764	90.6	1.84	0.430	0.791
7	4.11	5.96	.0760	91.2	3.15	0.430	1.354
8	4.15	5.98	.0755	90.4	2.65	0.430	1.139
9	4.15	5.98	.0759	90.4	2.17	0.430	0.933
10	4.03	5.97	.1073	92.4	2.29	0.430	0.985
11	4.05	5.98	.1076	92.1	4.55	0.430	1.957
12	4.06	5.99	.1080	92.0	6.29	0.430	2.705
13	4.05	5.98	.1078	91.7	3.82	0.4125	1.576
14	4.15	5.98	.1076	90.0	5.24	0.4125	2.161
15	4.29	5.98	.1081	89.2	5.80	0.4125	2.392

NOTE: Specimens numbered 1-5 correspond to specimens numbered 4-8 and specimens numbered 6-9 correspond to those numbered 10-13 of reference (6).

TABLE II-1b

DATA FOR HOT-ROLLED MILD STEEL SPECIMENS

Spec. No.	δ_m in	δ_o in	δ_o/H_s	V_o in/sec	λ	$\lambda(H_s/R)$	ER
1	.0960	.0960	0.7960	3308	62.5	3.67	63.8
2	.1722	.1703	1.4121	4355	107.8	6.34	110.5
3	.0470	.0470	0.3910	2346	31.0	1.83	32.2
4	.1020	.1020	0.8437	3474	67.3	4.00	70.5
5	.1481	.1481	1.2290	4013	92.2	5.40	93.9
6	.0273	.0273	0.3573	2046	63.3	2.34	26.1
7	.1272	.1135	1.4934	3518	186.4	6.89	77.7
8	.0905	.0844	1.1179	2984	138.6	5.04	55.6
9	.0480	.0480	0.6324	2431	90.0	3.33	36.9
10	.0259	.0259	1.2414	1789	22.4	1.19	18.9
11	.1021	.1021	0.9489	3548	88.3	4.69	74.0
12	.2096	.2096	1.9407	4888	167.2	8.90	140.0
13	.0664	.0664	0.6160	2852	56.9	3.03	48.0
14	.1182	.1182	1.0985	3910	112.7	5.84	90.0
15	.1535	.1535	1.4200	4361	148.3	7.47	107.9

TABLE II-2a

DATA FOR 6061-T6 ALUMINUM SPECIMENS

Spec. No.	D in	2L in	H_s in	θ deg	W_e gm	I_o lb-sec/gm	I lb-sec
1	4.12	5.98	.1244	90.0	1.34	0.430	0.576
2	4.07	5.95	.1248	91.2	2.11	0.430	0.907
3	4.10	5.98	.1248	90.2	2.64	0.430	1.135
4	4.11	5.99	.1249	90.1	2.44	0.430	1.049
5	4.15	5.98	.0818	90.4	1.35	0.430	0.581
6	4.15	5.98	.0815	90.4	1.81	0.430	0.778
7	4.14	5.97	.0815	90.7	1.57	0.430	0.675
8	4.11	5.98	.0816	91.2	1.20	0.430	0.516
9	4.14	5.98	.0816	90.6	1.67	0.430	0.718
10	4.06	5.95	.0906	92.7	1.25	0.4125	0.516
11	4.06	5.96	.0910	92.1	1.40	0.4125	0.577
12	4.06	5.96	.0909	92.5	1.59	0.4125	0.656
13	4.18	5.97	.0909	90.0	1.33	0.4125	0.549
14	4.06	5.97	.0908	92.0	1.13	0.4125	0.466
15	4.13	5.96	.0908	90.8	2.31	0.4125	0.953

NOTE: Specimens numbered 1-4 correspond to specimens numbered 5-8 and specimens numbered 5-9 correspond to those numbered 10-14 of reference (6).

TABLE II-2b

DATA FOR 6061-T6 ALUMINUM SPECIMENS

Spec. No.	δ_m in	δ_o in	δ_o/H_s	V_o in/sec	λ	$\lambda(H_{s/R})$	ER
1	.0212	.0212	0.1704	2610	11.3	0.68	3.8
2	.0633	.0633	0.5072	4086	27.0	1.65	9.5
3	.0995	.0995	0.7973	5120	42.9	2.61	14.8
4	.0930	.0930	0.7446	4730	36.8	2.23	12.6
5	.0652	.0637	0.7787	4052	67.4	2.66	10.0
6	.1410	.1410	1.7301	5453	122.9	4.83	18.0
7	.1002	.0962	1.1804	4728	92.0	3.62	13.6
8	.0557	.0557	0.6826	3605	52.6	2.09	7.9
9	.1107	.1068	1.3088	5023	103.6	4.08	15.3
10	.0281	.0219	0.2417	3229	32.3	1.44	6.0
11	.0441	.0441	0.4846	3601	39.8	1.78	7.5
12	.0664	.0659	0.7250	4094	51.6	2.31	9.6
13	.0340	.0322	0.3542	3441	38.6	1.68	6.7
14	.0175	.0115	0.1267	2913	26.2	1.17	4.9
15	TOTAL SHEAR ALONG CLAMPED EDGE						

TABLE II-3

PERMANENT DEFLECTION DATA

FOR HOT-ROLLED MILD STEEL SPECIMENS

Deflections are in inches. See figure II-8 for x,y coordinates.

a. Mild Steel Specimen No. 10

y \ x	1	2	3	4	5
1	.0080	.0112	.0133	.0109	.0074
2	.0179	.0223	.0220	.0212	.0160
3	.0228	.0252	.0259*	.0236	.0220
4	.0180	.0200	.0209	.0199	.0166
5	.0077	.0117	.0136	.0993	.0105

* Denotes maximum deflection

TABLE II-3 (Continued)

b. Mild Steel Specimen No. 11

y \ x	1	2	3	4	5
1	.0124	.0364	.0374	.0294	.0053
2	.0337	.0806	.0786	.0757	.0259
3	.0444	.0905	.1021*	.0768	.0464
4	.0324	.0817	.0849	.0720	.0303
5	.0086	.0306	.0360	.0301	.0120

TABLE II-3 (Continued)

c. Mild Steel Specimen No. 12

y \ x	1	2	3	4	5
1	.0200	.0612	.0839	.0714	.0213
2	.0590	.1417	.1669	.1576	.0506
3	.0769	.1675	.2096*	.1870	.0715
4	.0594	.1586	.1941	.1823	.0572
5	.0170	.0863	.0980	.1007	.0248

TABLE II-3 (Continued)

d. Mild Steel Specimen No. 13

y \ x	1	2	3	4	5
1	.0258	.0281	.0535	.0325	.0218
2	.0316	.0645	.0635	.0562	.0252
3	.0388	.0640	.0664*	.0573	.0334
4	.0213	.0349	.0245	.0261	.0186
5	.0090	.0211	.0289	.0202	.0119

TABLE II-3 (Continued)

e. Mild Steel Specimen No. 14

y \ x	1	2	3	4	5
1	.0116	.0384	.0488	.0466	.0136
2	.0403	.0975	.1030	.0970	.0421
3	.0506	.1060	.1182*	.1114	.0588
4	.0385	.0990	.1126	.1079	.0457
5	.0097	.0522	.0629	.0542	.0170

TABLE II-3 (Continued)

f. Mild Steel Specimen No. 15

y \ x					
1	.0121	.0524	.0594	.0535	.0134
2	.0367	.1179	.1308	.1165	.0374
3	.0473	.1289	.1535*	.1327	.0488
4	.0353	.1083	.1300	.1188	.0385
5	.0115	.0492	.0620	.0548	.0131

TABLE II-4

PERMANENT DEFLECTION DATA FOR 6061-T6 ALUMINUM SPECIMENS

Deflections are in inches. See figure II-8 for x,y coordinates.

a. 6061-T6 Aluminum Specimen No. 10

x \ y	1	2	3	4	5
1	.0011	.0013	.0036	.0056	.0037
2	.0016	.0048	.0077	.0064	.0071
3	.0011	.0075	.0103	.0142	.0063
4	.0043	.0149	.0176	.0261	.0098
5	.0077	.0170	.0229	.0281*	.0166
6	.0095	.0176	.0219	.0262	.0144
7	.0106	.0220	.0239	.0277	.0132
8	.0116	.0193	.0226	.0263	.0172
9	.0030	.0107	.0120	.0152	.0058
10	.0023	.0031	.0054	.0060	.0022
11	.0006	.0021	.0042	.0041	.0022

* Denotes Maximum deflection

TABLE II-4 (Continued)

b. 6061-T6 Aluminum Specimen No. 11

x \ y	1	2	3	4	5
1	.0017	.0033	.0055	.0072	.0025
2	.0041	.0062	.0078	.0066	.0048
3	.0103	.0143	.0163	.0184	.0169
4	.0190	.0308	.0329	.0400	.0322
5	.0181	.0335	.0436	.0417	.0344
6	.0213	.0346	.0441*	.0428	.0254
7	.0193	.0345	.0417	.0409	.0270
8	.0186	.0313	.0319	.0354	.0244
9	.0123	.0153	.0165	.0192	.0134
10	.0057	.0053	.0072	.0071	.0058
11	.0062	.0021	.0039	.0033	.0057

c. 6061-T6 Aluminum Specimen No. 12

x \ y	1	2	3	4	5
1	.0019	.0051	.0076	.0077	.0064
2	.0034	.0105	.0120	.0118	.0066
3	.0161	.0263	.0254	.0258	.0164
4	.0339	.0400	.0500	.0435	.0282
5	.0414	.0598	.0633	.0620	.0306
6	.0432	.0640	.0659	.0610	.0316
7	.0422	.0567	.0664*	.0618	.0296
8	.0293	.0509	.0512	.0560	.0265
9	.0148	.0234	.0277	.0270	.0202
10	.0042	.0074	.0124	.0114	.0097
11	.0023	.0066	.0086	.0105	.0045

TABLE II-4 (Continued)

d. 6061-T6 Aluminum Specimen No. 13

x \ y	1	2	3	4	5
1	.0003	.0033	.0050	.0050	.0024
2	.0057	.0055	.0069	.0043	.0046
3	.0109	.0146	.0146	.0135	.0105
4	.0184	.0261	.0268	.0300	.0187
5	.0237	.0297	.0303	.0317	.0198
6	.0272	.0310	.0322	.0282	.0191
7	.0294	.0340*	.0257	.0302	.0205
8	.0265	.0333	.0331	.0308	.0187
9	.0185	.0195	.0188	.0172	.0110
10	.0118	.0097	.0099	.0060	.0059
11	.0101	.0081	.0080	.0049	.0051

TABLE II-4 (Continued)

e. 6061-T6 Aluminum Specimen No. 14

x \ y	1	2	3	4	5
1	.0044	.0054	.0054	.0047	.0033
2	.0036	.0056	.0059	.0056	.0037
3	.0060	.0086	.0084	.0096	.0078
4	.0099	.0146	.0150	.0169	.0130
5	.0074	.0138	.0152	.0175*	.0121
6	.0066	.0094	.0115	.0126	.0111
7	.0053	.0090	.0100	.0123	.0095
8	.0059	.0081	.0087	.0126	.0084
9	.0041	.0049	.0053	.0070	.0044
10	.0027	.0031	.0033	.0033	.0028
11	.0017	.0022	.0023	.0021	.0015

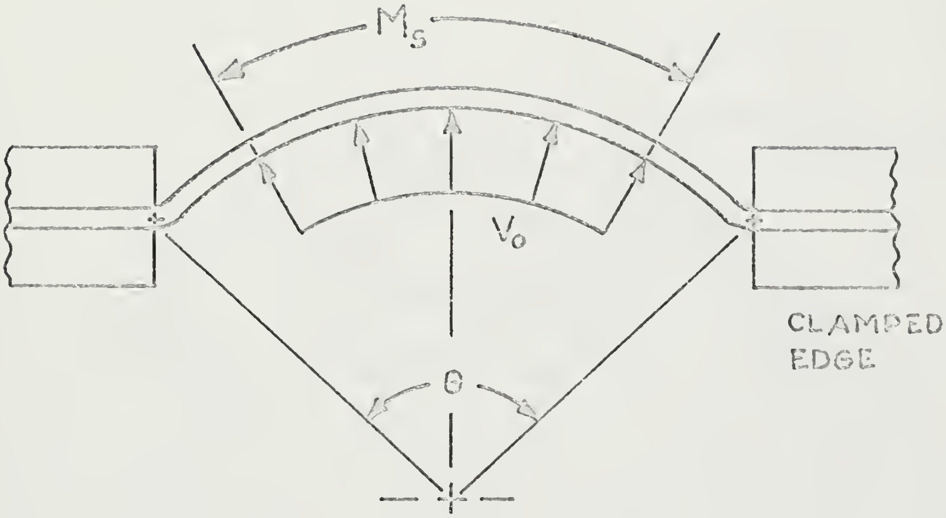

SPECIMEN MASS, M_S

FIGURE II-1

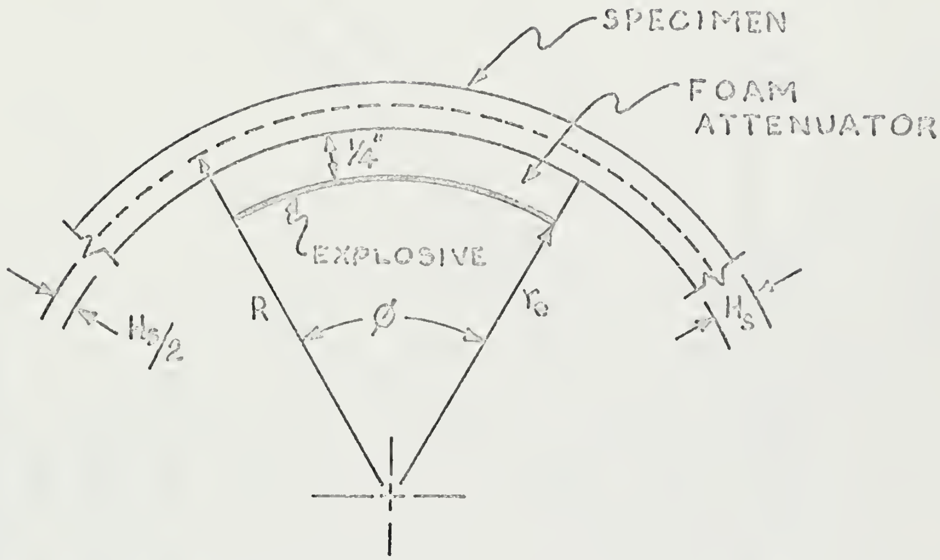

FIGURE II-2

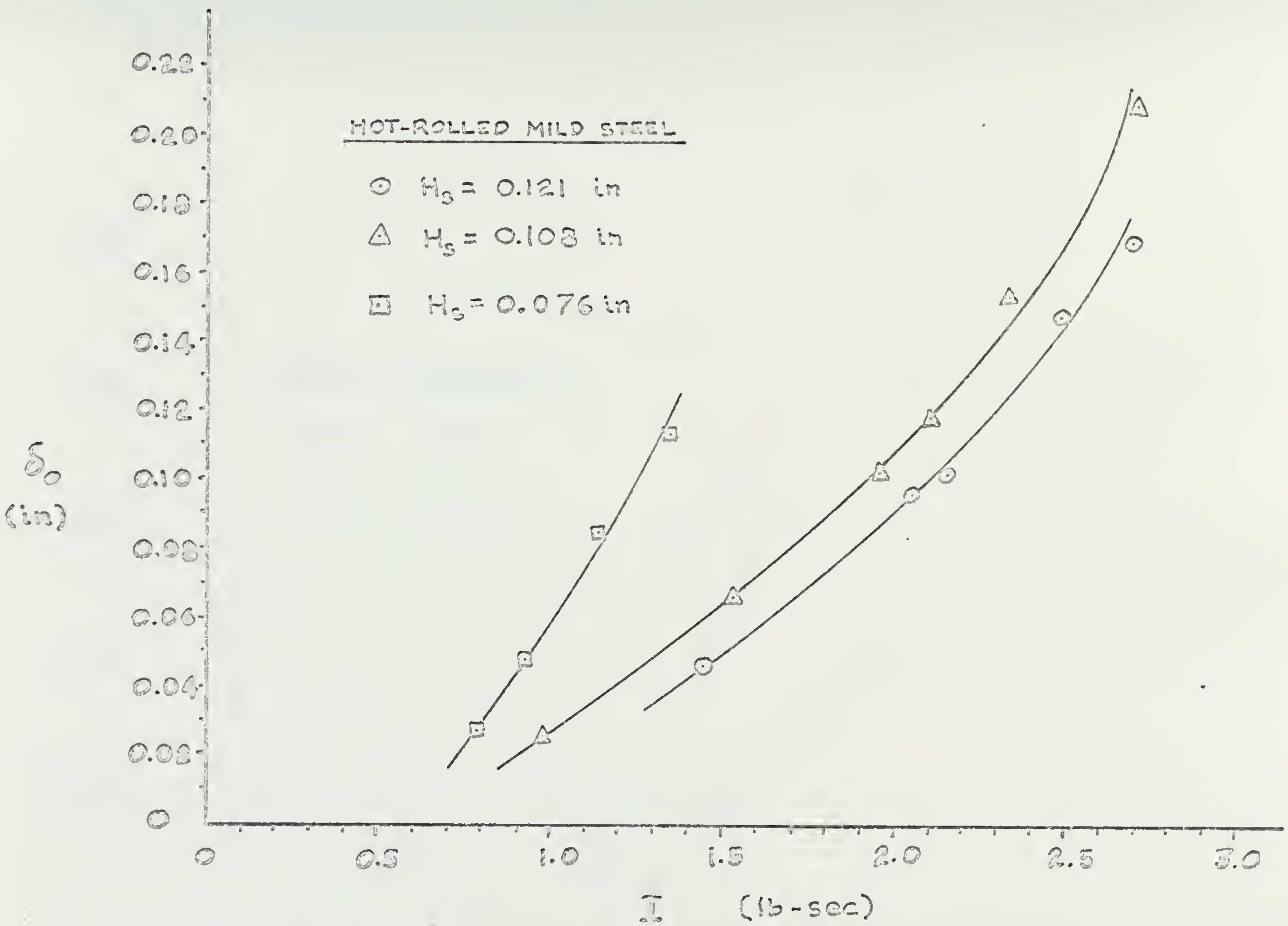
HOT-ROLLED MILD STEEL
⊙ H_s = 0.121 in
△ H_s = 0.108 in
⊡ H_s = 0.076 in
δ_o (in)
0
0.02
0.04
0.06
0.08
0.10
0.12
0.14
0.16
0.18
0.20
0.22
0
0.5
1.0
1.5
2.0
2.5
3.0
I (lb-sec)

FIGURE II - 3

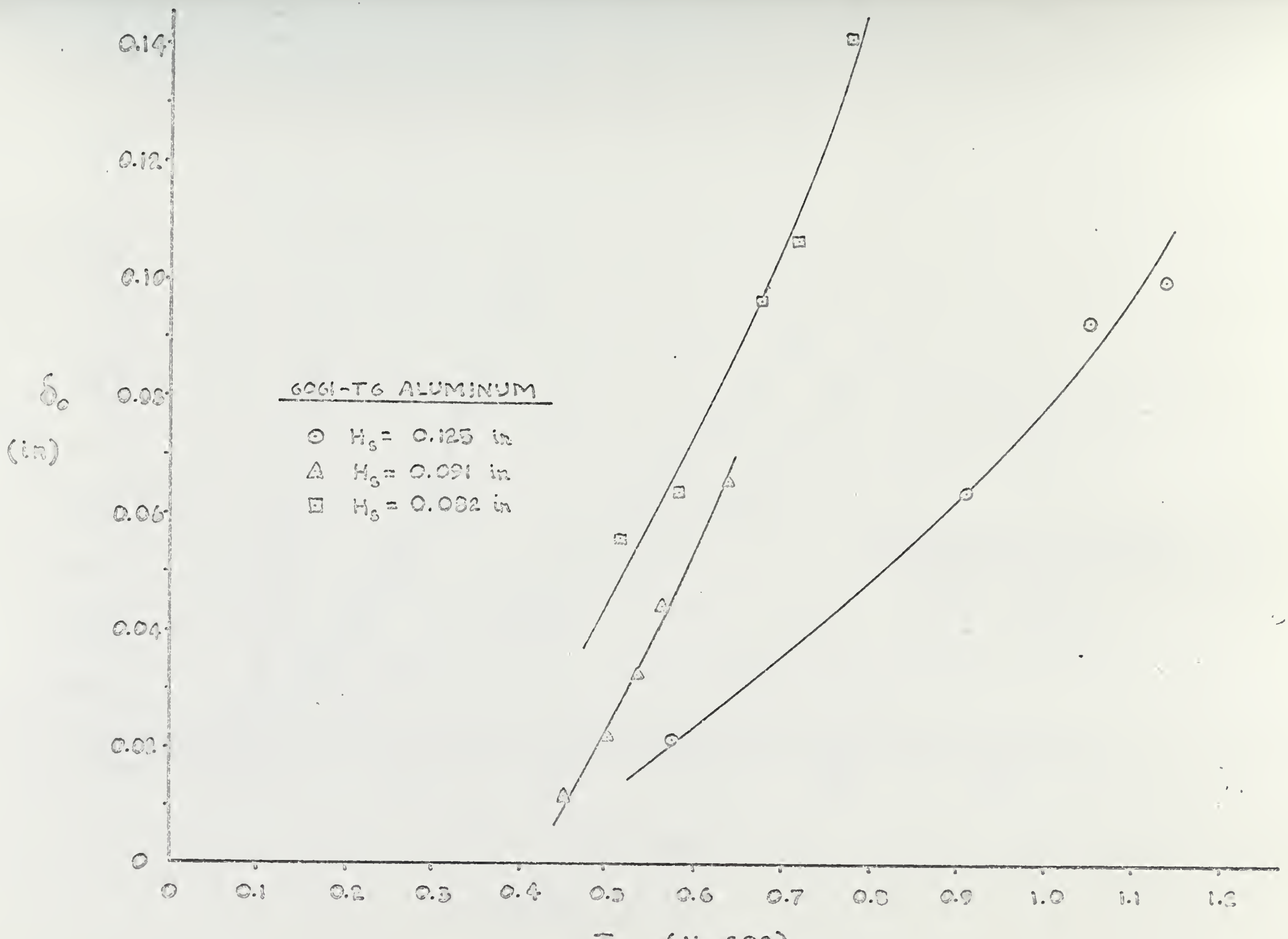
6061-T6 ALUMINUM
⊙ H_s = 0.125 in
△ H_s = 0.091 in
⊡ H_s = 0.082 in
δ_c (in)
0.14
0.12
0.10
0.08
0.06
0.04
0.02
0
0 0.1 0.2 0.3 0.4 0.5 0.6 0.7 0.8 0.9 1.0 1.1 1.2
I (lb-sec)

FIGURE II-4

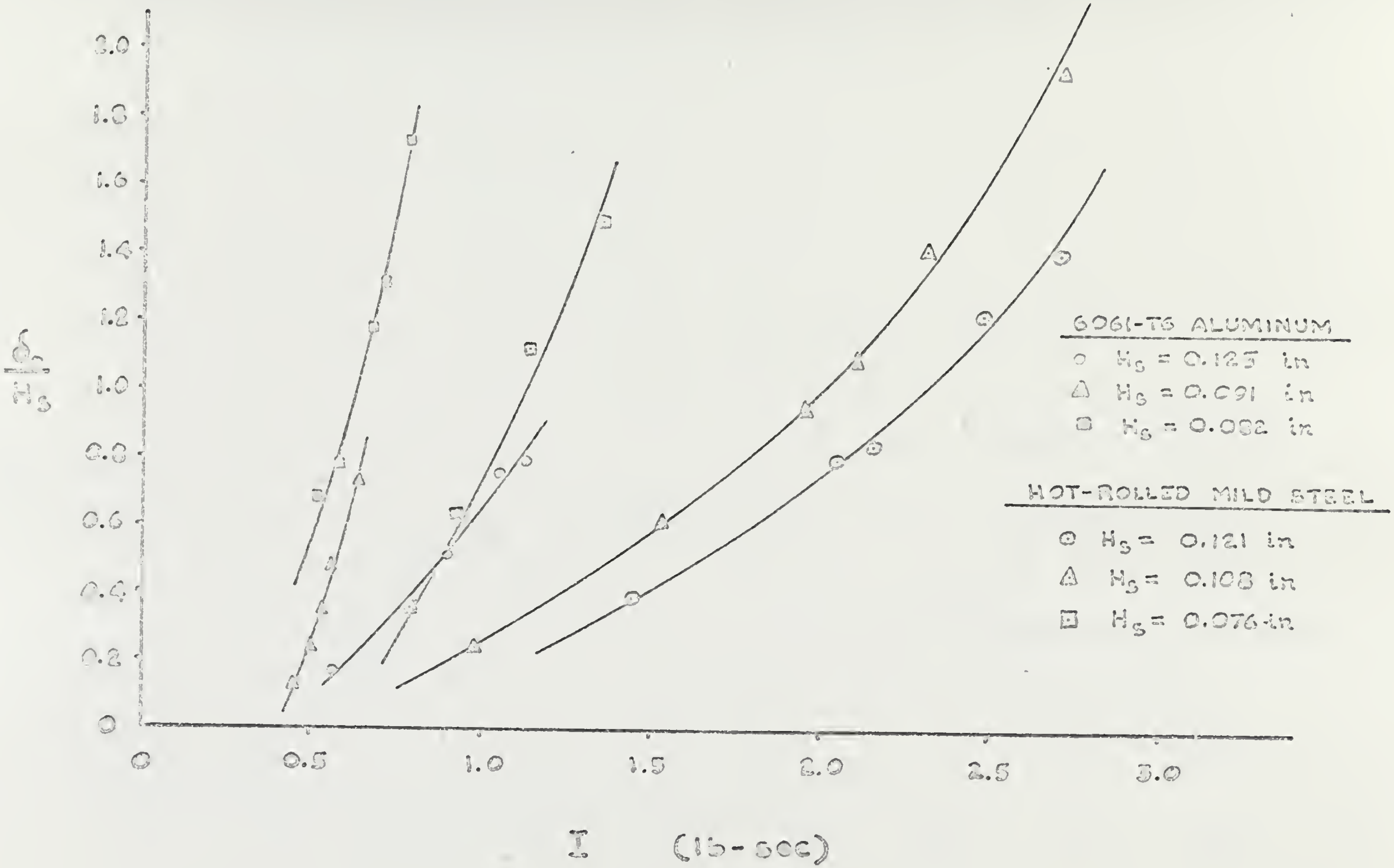

δ / Hs
3.0
1.8
1.6
1.4
1.2
1.0
0.8
0.6
0.4
0.2
0
0
0.5
1.0
1.5
2.0
2.5
3.0
I (lb-sec)
6061-T6 ALUMINUM
○ Hs = 0.125 in
△ Hs = 0.091 in
□ Hs = 0.082 in
HOT-ROLLED MILD STEEL
⊙ Hs = 0.121 in
△ Hs = 0.108 in
⊡ Hs = 0.076 in

FIGURE II-5

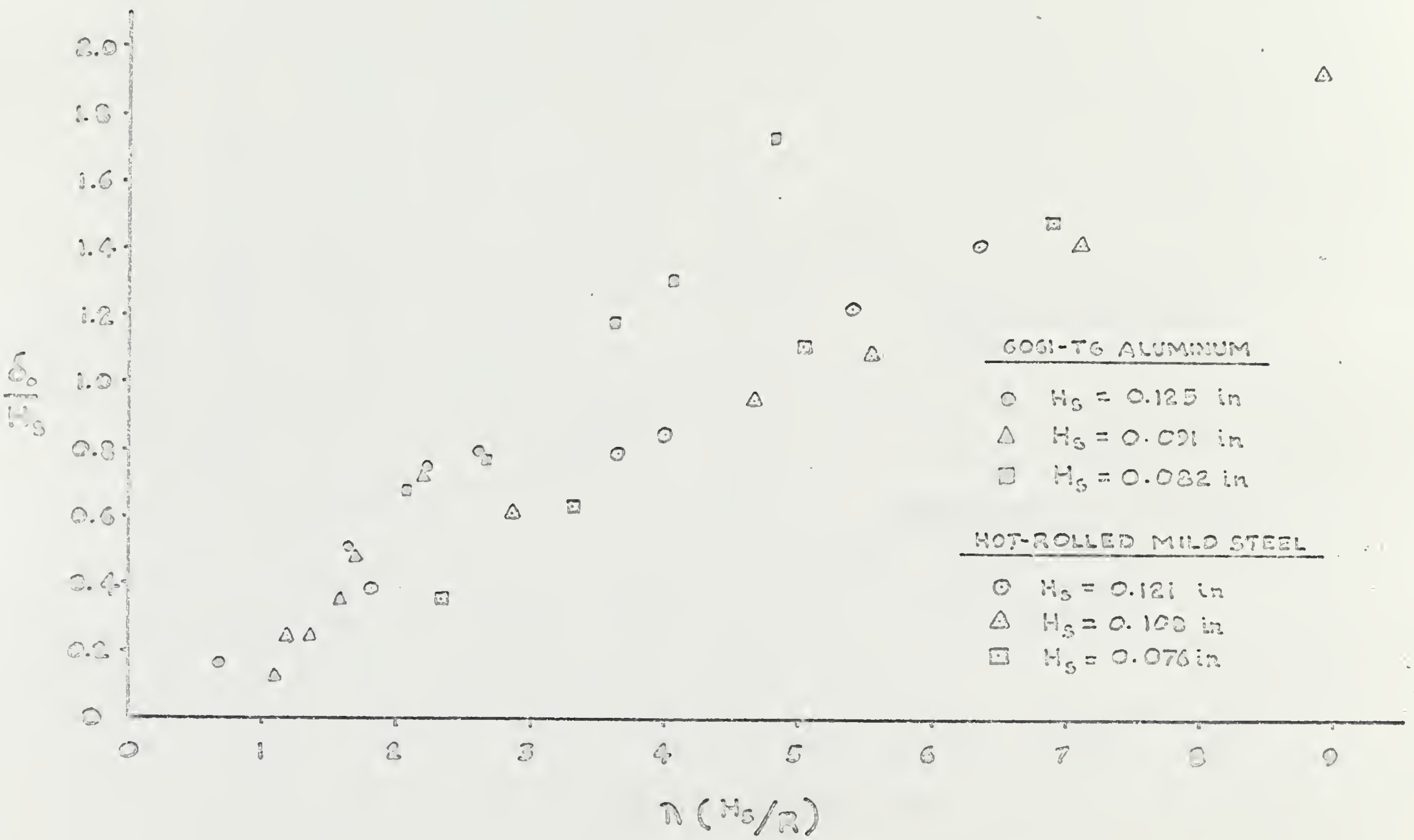

2.0
1.8
1.6
1.4
1.2
1.0
0.8
0.6
0.4
0.2
0
0
1
2
3
4
5
6
7
8
9
6061-T6 ALUMINUM
Hs = 0.125 in
Hs = 0.091 in
Hs = 0.082 in
HOT-ROLLED MILD STEEL
Hs = 0.121 in
Hs = 0.100 in
Hs = 0.076 in

FIGURE II-6

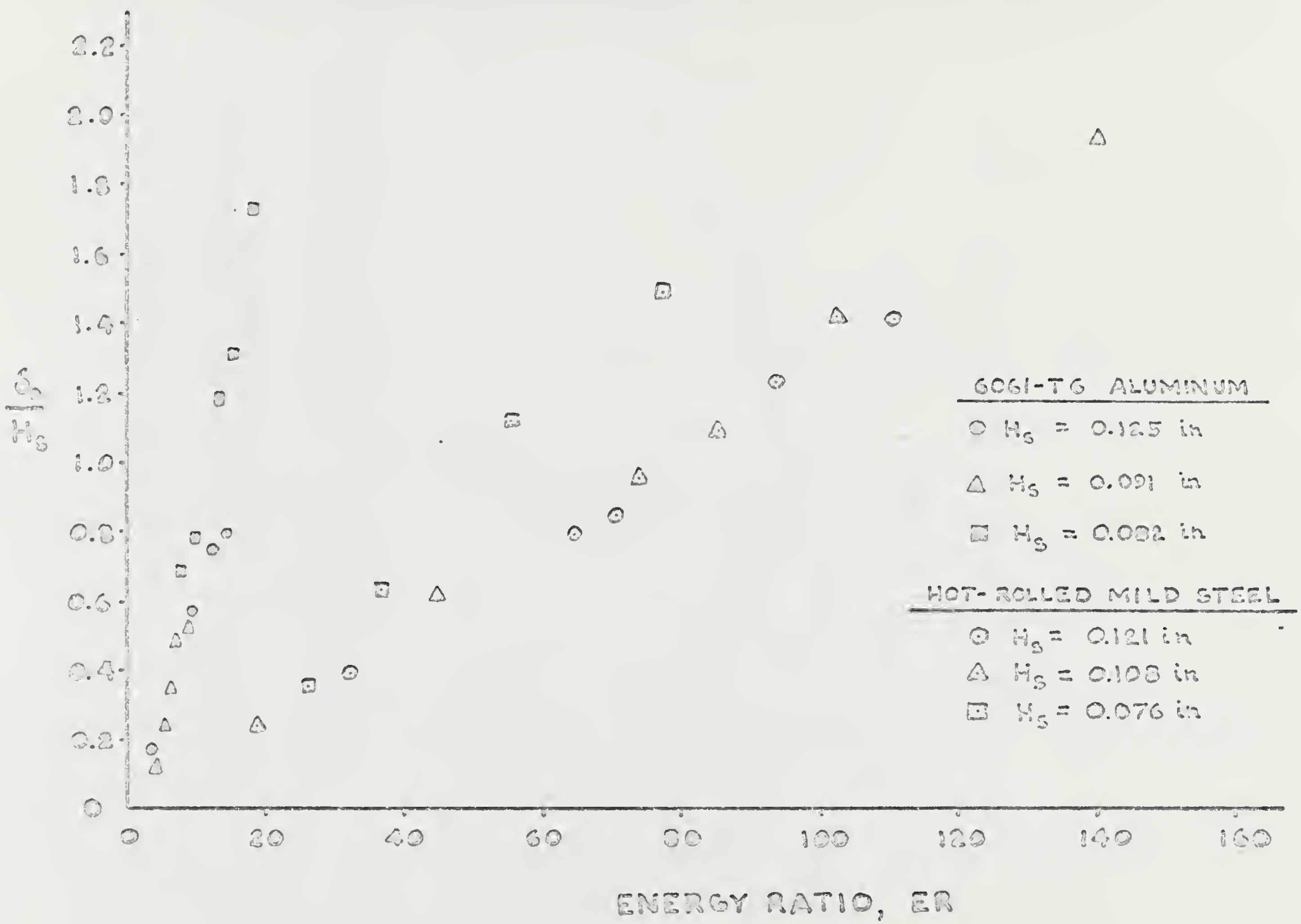
6061-T6 ALUMINUM
○ H_s = 0.125 in
△ H_s = 0.091 in
□ H_s = 0.082 in
HOT-ROLLED MILD STEEL
⊙ H_s = 0.121 in
△ H_s = 0.108 in
⊡ H_s = 0.076 in
δ / H_s
0
0.2
0.4
0.6
0.8
1.0
1.2
1.4
1.6
1.8
2.0
2.2
0
20
40
60
80
100
120
140
160
ENERGY RATIO, ER

FIGURE II-7

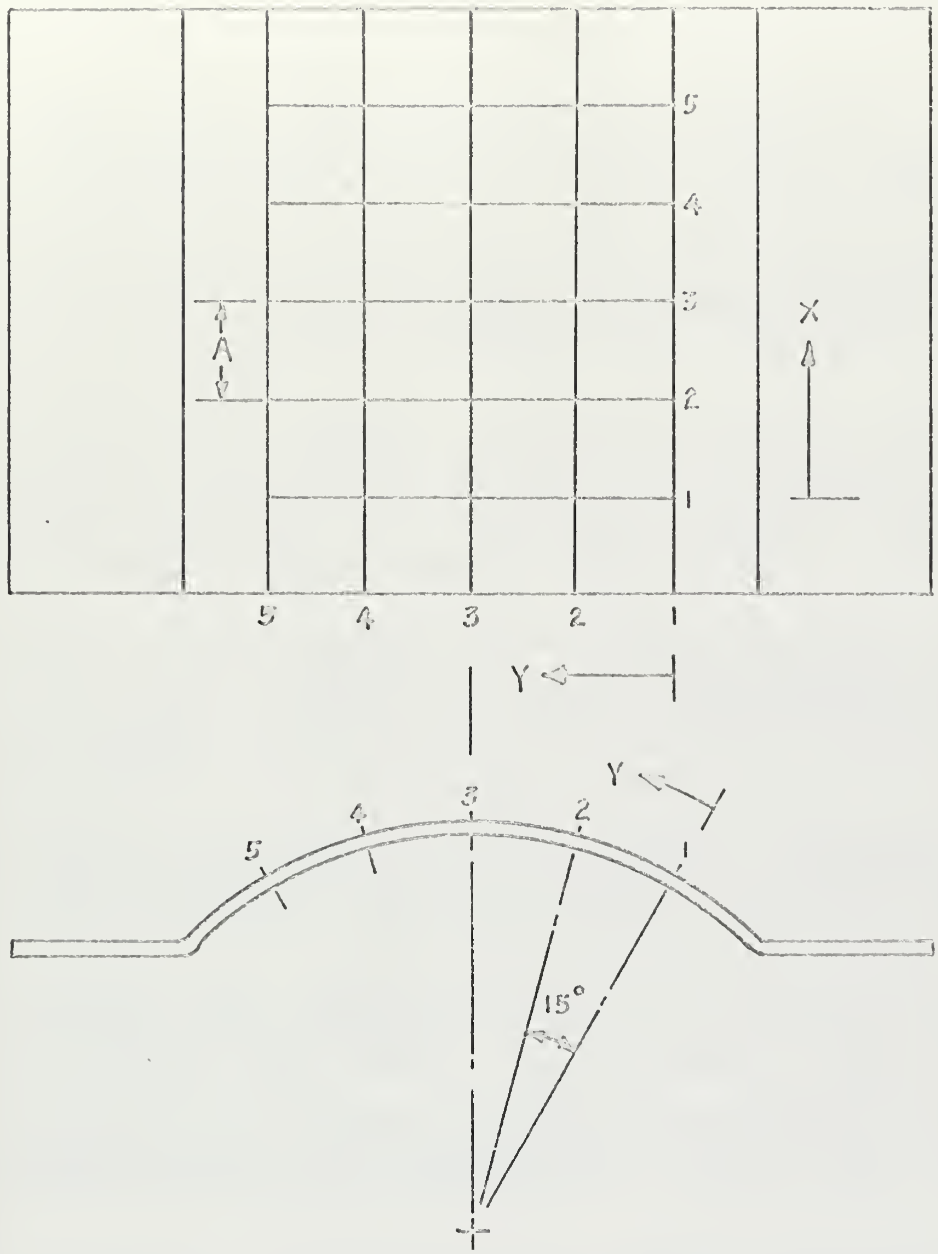

NOTE: A = 1 INCH FOR MILD STEEL PANELS
A = 1/2 INCH FOR 6061-T6 ALUMINUM PANELS

COORDINATE SYSTEM
90 DEGREE CYLINDRICAL PANELS

FIGURE II-8

REFERENCES

1. Baker, W.E., "The Elastic-Plastic Response of Thin Spherical Shells to Internal Blast Loading", Journal of Applied Mechanics, pp. 139-144, March, 1960.

2. Bodner, S.R. and Symonds, P.S., "Experimental and Theoretical Investigation of Plastic Deformation of Cantilever Beams Subjected to Impulsive Loading", Journal of Applied Mechanics, Vol. 29, 1962, pp. 719-728.

3. Clark, E.N., Schmitt, F.H., and Juriaco, I.P., "Plastic Deformation of Structures, Part III, Large Plastic Deformation of Clamped Cylindrical Panels", AFFDL-TDR 64-64 Vol. III, Engineering Sci. Lab, Picatinny Arsenal, Dover, N.J., 1968.

4. Clark, E.N., Schmitt, F.H., Ellington, D.G., Engle, I.A., and Nicolaides, S., "Plastic Deformation of Structures: Volume I - Plastic Deformation Beams.", Air Force Flight Dynamics Laboratory, FOL-TDR-64-64, May 1965.

5. Duffey, T., "Significance of Strain Hardening and Strain Rate Effects on the Transient Responses of Elastic-Plastic Spherical Shells", Research Report SC-RR-69-477, Sandia Laboratories, September 1969.

6. Dumas, J.W., "Dynamic Response of Cylindrical Shells to Impulsive Loading", Thesis, M.S. in Naval Arch. and Marine Eng., Mass. Inst. of Tech., June 1970.

7. Duszek, M., "Plastic Analysis of Cylindrical Shells Subjected to Large Deflections", Arch. Mech. Stos. Vol. 18, 1966, pp. 599-614.

8. Eason, G., and Shield, R.T., "Dynamic Loading of Rigid-Plastic Cylindrical Shells", Journal of Mech. Phys. Solids, Vol. 4, pp. 53-71, 1956.

9. Florence, A.L., "Buckling of Viscoplastic Cylindrical Shells Due to Impulsive Loading", AIAA Journal Vol. 6, No. 3, March 1968.

10. Giannotti, J.G., "An Experimental Study Into the Dynamic Behavior of Spherical Shells", Thesis, M.S. in Civil Eng., Mass. Inst. of Tech., June 1970.

11. Hodge, P.G., "The Influence of Blast Characteristics on the Final Deformation of Circular Cylindrical Shells", Journal of Applied Mechanics, Vol. 23, 1956 Trans. ASME, Vol. 78, pp. 617-624.

12. Hodge, P.G., and Paul, B., "Approximate Yield Conditions in Dynamic Plasticity", Proc. Third Midwestern Conference on Solid Mechanics, 1957, pp. 29-47.

13. Hodge, P.G., "Impact Pressure Loading of Rigid-Plastic Cylindrical Shells", Journal of Mech. Phys. Solids, 1955, Vol. 3, pp. 176-188.

14. Hodge, P.G., "Effect of End Conditions on Dynamic Loading of Plastic Shells", Journal of Mech. Phys. Solids, Vol. 7 No. 4, October 1959, pp. 258-263.

15. Humphreys, J.S., "Plastic Deformation of Impulsively Loaded Straight Clamped Beams", Jour. App. Mechs., Vol. 32, No. 1, 1965, pp. 7-10.

16. Jones, N., Griffin, R.N., and Van Duzer, R.N., "An Experimental Study into the Dynamic Plastic Behavior of Wide Beams and Rectangular Plates", Report No. 69-12, M.I.T., Department of Naval Architecture and Marine Engineering, October, 1969.

17. Jones, N., Uran, T.O., and Tekin, S.A., "The Dynamic Behavior of Fully Clamped Rectangular Plates", International Journal of Solids and Structures, Vol. 6, pp. 1499-1512, 1970.

18. Jones, N., "Influence of Strain Hardening and Strain Rate Sensitivity on the Permanent Deformation of Impulsively Loaded Rigid-Plastic Beams", International Journal of Mechanical Sciences, Vol. 9, pp. 777-796, 1967.

19. Jones, N., "Finite Deflections of a Rigid-Viscoplastic Strain Hardening Annular Plate Loaded Impulsively", Journal of Applied Mechanics, Vol. 35, No. 2, pp. 349-356, 1968.

20. Jones, N., "The Influence of Large Deflections on the Behavior of Rigid-Plastic Cylindrical Shells Loaded Impulsively", Journal of Applied Mechanics, Vol. 37, No. 2, pp. 416-425, 1970.

21. Jones, N., "An Approximate Rigid-Plastic Analysis of Shell Intersections Loaded Dynamically" Report No. 70-20, M.I.T., Department of Naval Architecture and Marine Engineering, October 1970.

22. Kuzin, P.A., and Shapiro, G.S., "On Dynamic Behavior of Plastic Structures", Ed. H. Gortler Proc. 11th International Cong. of App. Mechs., Munich 1964, Springer-Verlag, pp. 629-635, 1966.

23. Leech, J.W., Witmer, E.A., and Pian, T.H.H., "A Numerical Calculation Technique for Large Elastic-Plastic Transient Deformations of Thin Shells", AIAA Journal, Vol. 6, No. 12, pp. 2352-2359, 1968.

24. Lock, M.H., Okubo, S., and Whittier, J.S., "Experiments on the Snapping of a Shallow Dome Under a Step Pressure Load", AIAA Journal, Vol. 6, No. 7, pp. 1320-1326, July, 1968.

25. Morino, L., Leech, J.W., and Witmer, E.A., "An Improved Numerical Calculation Technique for Large Elastic-Plastic Transient Deformation of Thin Shells", Applied Mechanics Conference, Report 25-21, 1969, University of New Mexico.

26. Parkes, E.W., "The Permanent Deformation of a Cantilever Struck Transversely at Its Tip", Proceedings of the Royal Society, London, Series A Vol. 228, 1955, pp. 462-476.

27. Sankaranarayanan, R., "On the Dynamics of Plastic Spherical Shells", Journal of Applied Mechanics, pp. 87-90, March, 1963.

28. Sankaranarayanan, R., "On the Impact Pressure Loading of a Plastic Spherical Cap", Journal of Applied Mechanics Vol. 33, pp. 704-706, September 1966.

29. Symonds, P.S., "Survey of Methods for Plastic Deformation of Structures Under Dynamic Loadings", Brown University Report BU/NSRDCC/1-67, June, 1967.

30. Ting, T.C.T., "Large Deformation of a Rigid Ideally Plastic Cantilever Beam", Journal of Applied Mechanics, Vol. 32, 1965, pp. 295-302.

31. Wierzbicki, T., "Impulsive Loading of a Spherical Container with Rigid-Plastic and Strain Rate Sensitive Material", Archiwum Mechaniki Stosowanej Vol. 15, 1963, pp. 775-790.

APPENDIX A

MECHANICAL PROPERTIES OF TEST SPECIMEN MATERIALS

Tensile tests on the specimen materials were conducted on an Instron testing machine. The cross-head speed of the machine was 0.1 in/min. in all cases.

Two tests were conducted on samples of plate used for forming the spheres and cylindrical panels. These tensile test specimens were taken from two directions in the plate perpendicular to each other. Two tensile test specimens were also made from the parent material used for the cylindrical nozzles. These were taken from the parent material in directions parallel to each other. A 2 inch gage length was used with 2.125 inch between the machine jaws in each case.

The yield stress found here is the 0.2% offset yield stress. The value of the yield stress used in the calculations is the average yield stress from the two tests. The ultimate tensile stress is the maximum stress that the material can sustain. This is the maximum point on the stress-strain curve.

Percent elongation is the ratio of the increase in gage length to the original gage length to the point of fracture. It is used to compare the ductility of materials.

The results of the tensile tests are given in

Tables A-1, A-2 and A-3. Figures A-1 and A-2 show stress-strain curves for sphere and cylindrical nozzles.

Densities were found by carefully weighing and measuring the volume of samples of the parent material using a water displacement method. These results are given in Table A-4.

TABLE A-1

MECHANICAL PROPERTIES 6061-T6 ALUMINUM

SPHERE - NOZZLE INTERSECTIONS

SPHERE

CROSS-SECTION AREA in^2	σ_o psi	σ_u psi	e %
0.062	41,129	46,290	11.50
0.062	40,807	45,565	11.25

σ_o AVERAGE = 40,968 psi

CYLINDRICAL NOZZLE

CROSS-SECTION AREA in^2	σ_o psi	σ_u psi	e %
0.064	40.469	44.531	11.30
0.064	40,312	44,531	11.35

σ_o AVERAGE = 40,390 psi

TABLE A-2

MECHANICAL PROPERTIES HOT-ROLLED MILD STEEL

90 DEGREE CYLINDRICAL PANELS

Nominal thickness inches	σ_{o_1} psi	σ_o psi	σ_u psi	e %
	36100		51600	35.0
0.120		36900		
	37700		54100	29.0
	36300		51000	31.0
0.108		36650		
	37000		52900	30.0
	33900		49500	28.0
0.076		35250		
	36600		52000	30.0

TABLE A-3

MECHANICAL PROPERTIES 6061-T6 ALUMINUM

90 DEGREE CYLINDRICAL PANELS

Nominal thickness inches	σ_{o_1} psi	σ_o psi	σ_u psi	e %
	40800		45100	17.0
0.125		41350		
	41900		45200	17.0
	40500		45000	17.5
0.09		40700		
	40900		45200	17.0
	38000		43300	16.5
0.080		39350		
	40700		45100	16.8

TABLE A-4

SPECIMEN MATERIAL DENSITIES

SPECIMEN	MATERIAL	DENSITY, $lbm\text{-}sec^2/in^4$
Sphere	6061-T6 Aluminum	2.495×10^{-4}
Cylindrical Nozzle	6061-T6 Aluminum	2.479×10^{-4}
Cylindrical Panel	6061-T6 Aluminum	2.51×10^{-4}
Cylindrical Panel	Hot-rolled mild steel	7.26×10^{-4}

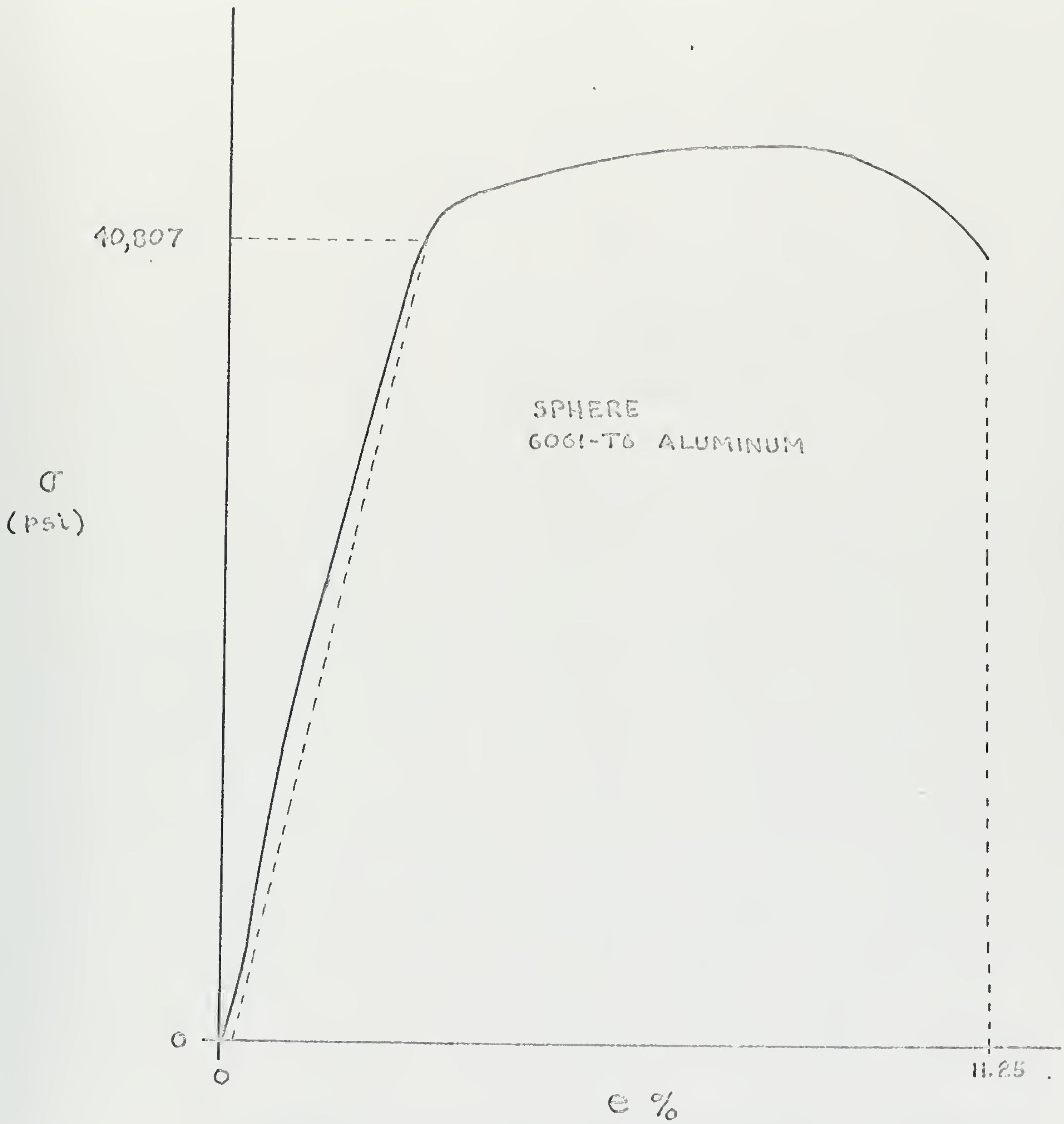

STRESS-STRAIN CURVE 6061-T6 ALUMINUM

FIGURE A-1

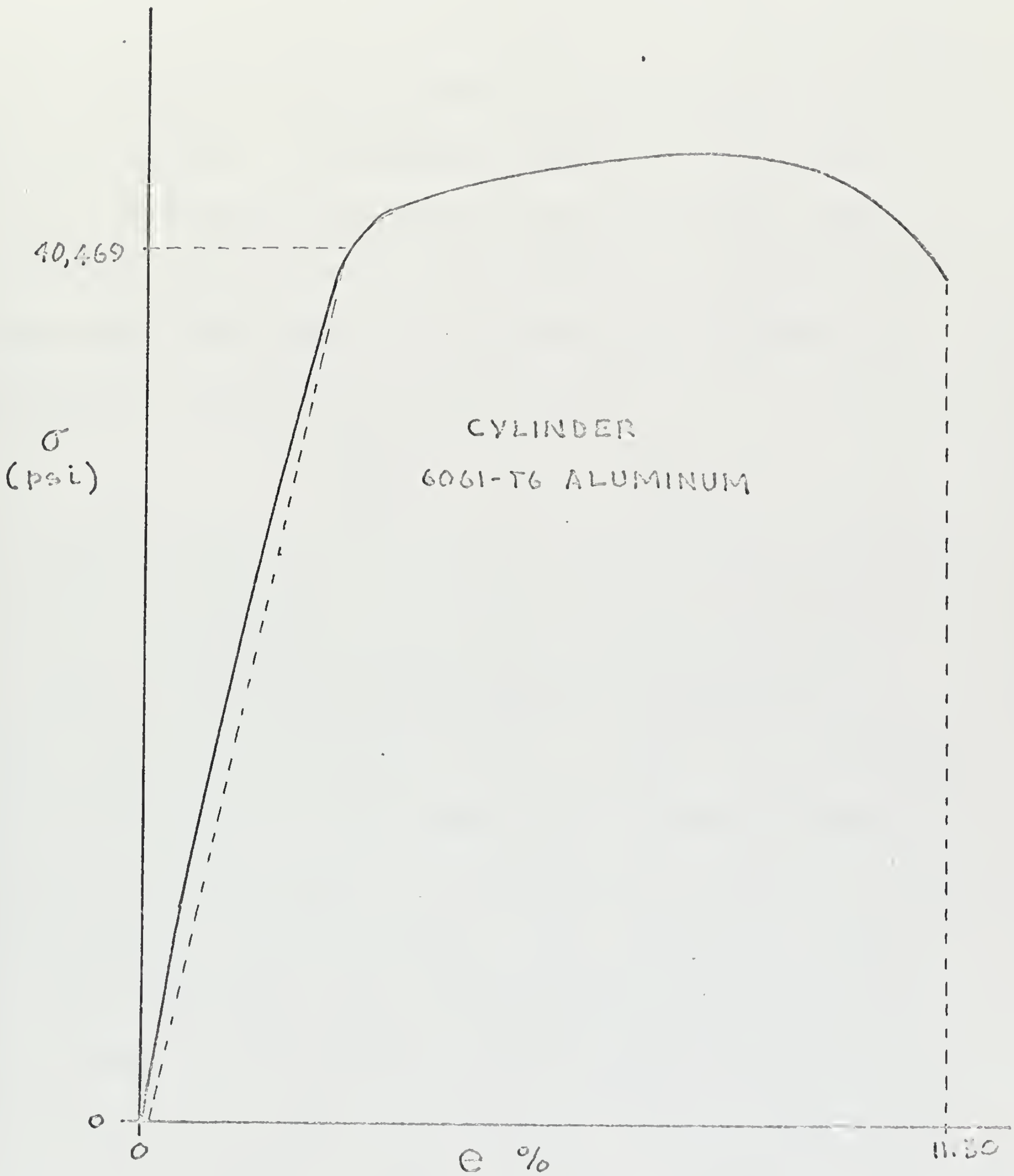

STRESS-STRAIN CURVE 6061-T6 ALUMINUM

FIGURE A-2.

APPENDIX B

EXPLOSIVE CALIBRATION TESTS

The specific impulse of the explosive was determined by a series of calibration tests which were independent of the tests conducted on the sphere-nozzle intersections or cylindrical panels. The general method of calibration was that of measuring the velocity of a circular disk which had been accelerated either upward or downward by the explosive. The specific impulse of the explosive is related to the measured velocity by:

$$I_o = \frac{M_s V_o}{W_e}$$

The test specimens for these tests were a 1/8 inch thick by 3 inch diameter mild steel circular plates.

Figure B-1 presents the general arrangement of apparatus for the calibration tests. Tests were conducted on disks accelerated in the upward and downward directions. The velocity of the disk was determined by using a Fastax (Wollensak WF-2) framing camera. The camera was focused on the edge of the disk and photographed over the first several inches of its flight. The disk was surrounded by a baffle plate 1/4 inch from its edge so that smoke would not obscure the camera's field of view. A layer of 1/4 inch thick polyeurethene foam was used as an attenuator between the disk surface and the explosive sheet. The explosive

and foam attenuator was cut to conform to the 3 inch diameter size of the disk. A 1/8 inch wide by 20 inch long "Detasheet" leader was used between the explosive and a No. 6 electric blasting cap. The leader was attached at the center of the explosive sheet.

The camera time scale was provided by standard Fastax time calibration pulses from a 1-KC frequency standard, lighting a glow tube. This light was photographed on the film and allowed a time calibration for the time between frames. This calibration showed the camera speed to be such that there were 0.1666 milli-seconds between frames. One-hundred-foot rolls of Eastman Negative Type 7224 film or Kodak Reversal Type 7278 film was used.

The camera was connected to the electric blast circuit which triggered the camera and the blast. The blast was delayed for 0.7 seconds after the circuit was triggered to allow the camera to obtain maximum speed before the blast occurred.

A graduated rule was mounted on the baffle plate parallel to the flight path of the disk. The rule was close enough to the disk to neglect paralax (1/16 inch).

Since the elapsed time between each frame of the film is 0.1666 milli-seconds, by counting the number of frames and measuring the distance the disk traveled using the graduated rule, the disk velocity over various

intervals is obtained. These results are then corrected for the influence of gravity to obtain final velocities, and from these, an average velocity found. The average velocity is used with the weight of the explosive and mass of the disk to compute the specific impulse for each test.

The specific impulse used for the calculations is the average specific impulse from the calibration tests. The test results are given in Tables B-1, B-2, and B-3.

TABLE B-1

EXPLOSIVE CALIBRATION TESTS IN UPWARD DIRECTION

a. Test No. 1

X in	t 10^{-3}	V_g cm/sec	V_x cm/sec
0.50	0.17	194.8	7664.9
0.55	0.17	201.9	8419.3
0.50	0.17	207.8	7677.9
0.40	0.17	212.2	6198.6
0.55	0.17	218.5	8435.9
0.60	0.17	225.8	9190.2
0.50	0.17	230.6	7700.7
0.45	0.17	235.9	6959.5

initial X = 7.10 in initial t = 2.04×10^{-3} sec

H_e in	W_e gm	W_s gm	Vavg cm/sec	I_o dyne-sec/gm
0.030	4.80	107.32	7780.9	17.39×10^4

Note: V_g calculated at end of each corresponding interval using $V_g = 2gX$ in cm/sec

TABLE B-1 (Continued)

b. Test No. 2

X in	t 10^{-3} sec	V_g cm/sec	V_x cm/sec
0.55	0.17	209.5	8426.9
0.65	0.17	216.9	9928.6
0.60	0.17	223.5	9187.9
0.65	0.17	230.6	9942.3
0.50	0.17	236.6	7706.7

initial X = 8.25 in   initial t = 2.38×10^{-3} sec

H_e in	W_e gm	W_s gm	Vavg cm/sec	I_o dyne-sec/gm
0.030	5.15	106.93	9038.5	18.77×10^4

TABLE B-1 (Continued)

c. Test No. 3

X in	t 10^{-3} sec	V_g cm/sec	V_x cm/sec
0.95	0.34	208.9	7305.6
0.55	0.17	215.4	8443.1
0.55	0.17	221.2	8448.9
0.60	0.17	228.1	9192.8
0.45	0.17	233.0	6956.6
0.55	0.17	238.2	8465.9

initial X = 7.75 in   initial t = 2.21×10^{-3} sec

H_e in	W_e gm	W_s gm	Vavg cm/sec	I_o dyne-sec/gm
0.030	5.09	107.13	8135.5	17.12×10^4

TABLE B - 1 (Continued)

d. Test No. 4

X in	t 10^{-3} sec	V_g cm/sec	V_x cm/sec
0.55	0.17	225.8	8453.5
0.55	0.17	231.8	8459.5
0.50	0.17	237.1	7707.7

initial X = 9.65 in initial t = 2.89×10^{-3} sec

W_c gm	W_e gm	W_s gm	Vavg cm/sec	I_o dyne-sec/gm
0.030	5.11	107.15	8206.9	17.21×10^4

e. Test No. 5

X in	t 10^{-3} sec	V_g cm/sec	V_x cm/sec
0.25	0.17	155.1	3890.4
0.30	0.17	160.4	4640.7
0.25	0.17	164.1	3899.4
0.20	0.17	167.2	3155.5
0.30	0.17	171.6	4653.9
0.30	0.17	176.0	4658.3
0.25	0.17	179.5	3914.8
0.20	0.17	182.3	3170.6

initial X = 4.60 in   initial t = 2.72×10^{-3} sec

H_e gm	W_e gm	W_s gm	Vavg cm/sec	I_o dyne-sec/gm
0.020	2.50	107.35	3997.9	17.15×10^4

TABLE B - 1 (Continued)

f. Test No. 6

X in	t 10^{-3}sec	V_g cm/sec	V_x cm/sec
0.30	0.17	164.1	4646.4
0.35	0.17	169.3	5398.7
0.25	0.17	173.0	3908.3
0.30	0.17	177.7	4660.0
0.25	0.17	180.0	3916.1
0.30	0.17	184.6	4666.9
0.35	0.17	189.5	5418.9
0.30	0.17	193.3	4675.6

initial λ = 5.10 in   initial t = 2.89×10^{-3} sec

H_e gm	W_e gm	W_s gm	Vavg cm/sec	I_o dyne-sec/gm
0.020	2.62	107.29	4661.4	19.09×10^4

g. Test No. 7

X in	t 10^{-3} sec	V_g cm/sec	V_x cm/sec
0.25	0.17	157.1	3892.4
0.30	0.17	162.0	4644.3
0.30	0.17	166.2	4648.5
0.35	0.17	171.6	5400.9
0.25	0.17	175.4	3910.7
0.30	0.17	179.5	4661.8
0.30	0.17	182.3	3917.6
0.35	0.17	187.9	5417.3
0.25	0.17	191.0	3926.3

initial X = 4.70 in   initial t = 2.72×10^{-3} sec

H_c gm	W_c gm	W_s gm	Vavg cm/sec	I_o dyne-sec/gm
0.020	2.58	107.30	4491.1	18.68×10^4

TABLE B - 1 (Continued)

h. Test No. 8

X in	t 10^{-3} sec	V_g cm/sec	V_x cm/sec
0.75	0.51	142.1	3877.4
0.60	0.51	152.0	3140.1
0.60	0.51	162.0	3150.1
0.60	0.51	171.2	3159.3
0.60	0.51	179.5	3167.6
0.75	0.51	189.5	3924.8
0.60	0.51	197.6	3185.7
0.75	0.51	206.7	3942.0
0.75	0.51	215.8	3951.1

initial X = 3.30 in   initial t = 2.55×10^{-3} sec

H_e gm	W_e gm	W_s gm	Vavg cm/sec	I_o dyne-sec/gm
0.015	2.01	107.15	3499.8	18.71×10^4

TABLE B - 1 (Continued)

I. Test No. 9

λ in	t 10^{-3} sec	V_g cm/sec	V_x cm/sec
0.60	0.51	136.5	3124.6
0.55	0.51	146.3	2885.4
0.60	0.51	156.5	3144.6
0.65	0.51	166.2	3403.4
0.55	0.51	174.9	2914.0
0.60	0.51	182.3	3170.4
0.60	0.51	191.0	3179.1
0.65	0.51	199.1	3436.3
0.60	0.51	206.7	3194.8

initial X = 3.15 in initial t = 2.55×10^{-3} sec

M_e gm	W_e gm	W_s gm	Vavg cm/sec	I_o dyne-sec/gm
0.015	1.95	107.23	3161.4	17.38×10^4

TABLE B-2

EXPLOSIVE CALIBRATION TESTS IN DOWNWARD DIRECTION

A. Test No. 1

λ in	t 10^{-3}sec	V_g cm/sec	V_x cm/sec
0.65	0.17	189.5	9513.3
0.60	0.17	197.6	8768.6
0.65	0.17	206.1	9496.7
0.65	0.17	213.9	9488.9
0.60	0.17	220.1	8746.1
0.65	0.17	227.2	9477.6

initial λ = 6.55 inch initial t = 2.04×10^{-3} sec

H_e in	W_e gm	W_s gm	Vavg cm/sec	I_o dyne-sec/gm
0.030	5.20	106.92	9248.5	19.01×10^4

Note: V_g calculated at end of each corresponding interval using V_g = $2 g\lambda$ in cm/sec.

TABLE B-2 (Continued

b. Test No. 2

X in	t 10^{-3} sec	V_g cm/sec	V_x cm/sec
0.60	0.17	196.8	8769.4
0.60	0.17	205.0	8761.2
0.55	0.17	211.1	7993.1
0.55	0.17	216.9	7987.3
0.60	0.17	229.2	8737.0

initial X = 7.15 inch   initial t = 2.21 x 10^{-3} sec

H_e in	W_e gm	W_s gm	Vavg cm/sec	I_o dyne-sec/gm
0.030	5.10	107.01	8449.6	17.73 x 10^4

TABLE B-2 (Continued)

c. Test No. 3

X in	t 10^{-3} sec	V_g cm/sec	V_x cm/sec
0.60	0.17	205.8	8760.4
0.60	0.17	212.5	8753.7
0.65	0.17	219.5	9483.3
0.60	0.17	225.8	8740.4

initial X = 7.80 inch   initial t = 2.38×10^{-3} sec

H_e in	W_e gm	W_s gm	Vavg cm/sec	I_o dyne-sec/gm
0.030	5.12	107.00	8936.9	18.67×10^4

TABLE B-2 (Continued)

d. Test No. 4

X in	t 10^{-3}sec	V_g cm/sec	V_x cm/sec
0.40	0.17	176.0	5793.0
0.40	0.17	184.1	5784.9
0.40	0.17	190.0	5779.0
0.40	0.17	196.2	5772.8

initial X = 5.80 inch   initial t = 3.40×10^{-3} sec

H_e in	W_e gm	W_s gm	Vavg cm/sec	I_o dyne-sec/gm
0.025	3.33	107.03	5782.4	18.58×10^4

e. Test No. 5

X in	t 10^{-3} sec	V_g cm/sec	V_x cm/sec
0.25	0.17	155.1	3578.7
0.25	0.17	160.0	3573.8
0.25	0.17	163.4	3570.4
0.25	0.17	167.2	3567.6
0.25	0.17	170.7	3563.1

initial X = 4.60 inch   initial t = 2.72×10^{-3} sec

H_e in	W_e gm	W_s gm	Vavg cm/sec	I_o dyne-sec/gm
0.015	2.12	107.03	3570.7	18.02×10^4

TABLE B-2 (Continued)

f. Test No. 6

X in	t 10^{-3} sec	V_g cm/sec	V_x cm/sec
0.30	0.17	157.1	4313.3
0.30	0.17	162.0	4308.4
0.30	0.17	166.2	4304.2
0.25	0.17	169.3	3564.5
0.30	0.17	174.0	4296.4

initial λ = 4.65 inch   initial t = 2.72×10^{-3} sec

H_e in	W_e gm	W_s gm	Vavg cm/sec	I_o dyne-sec/gm
0.020	2.60	107.0	4157.4	17.11×10^4

TABLE B-3

EXPLOSIVE CALIBRATION TEST RESULTS

a. Upward Tests

Test No.	H_e in	$I_o \times 10^{-4}$ dyne-sec/gm
1	0.030	17.39
2	0.030	18.77
3	0.030	17.12
4	0.030	17.21
5	0.020	17.15
6	0.020	19.09
7	0.020	18.68
8	0.015	18.71
9	0.015	17.38

I_o average $= 17.94 \times 10^4$ dyne-sec/gm

This value must be corrected as t of 1.7×10^{-3} sec was used instead of $t = 1.666 \times 10^{-3}$ sec.

$$I_{o_u} = 17.94 \times 10^4 \times \frac{1.7}{1.666} = 18.30 \times 10^4 \text{ dyne-sec/gm}$$

TABLE B-3 (Continued)

b. Downward Tests

Test No.	H_c in	$I_o \times 10^{-4}$ dyne-sec/gm
1	0.030	19.01
2	0.030	17.73
3	0.030	18.67
4	0.025	18.58
5	0.015	18.02
6	0.020	17.11

I_o average $= 18.18 \times 10^4$ dyne-sec/gm

This value must be corrected as t of 1.7×10^{-3} sec was used instead of $t = 1.666 \times 10^{-3}$ sec.

$$I_{o_d} = 18.18 \times 10^4 \times \frac{1.7}{1.666} = 18.54 \times 10^4$$

$$I_o = \frac{I_{o_u} + I_{o_d}}{2} = 18.42 \times 10^4 \text{ dyne-sec/gm}$$

OR $= 0.4125$ lb-sec/gm

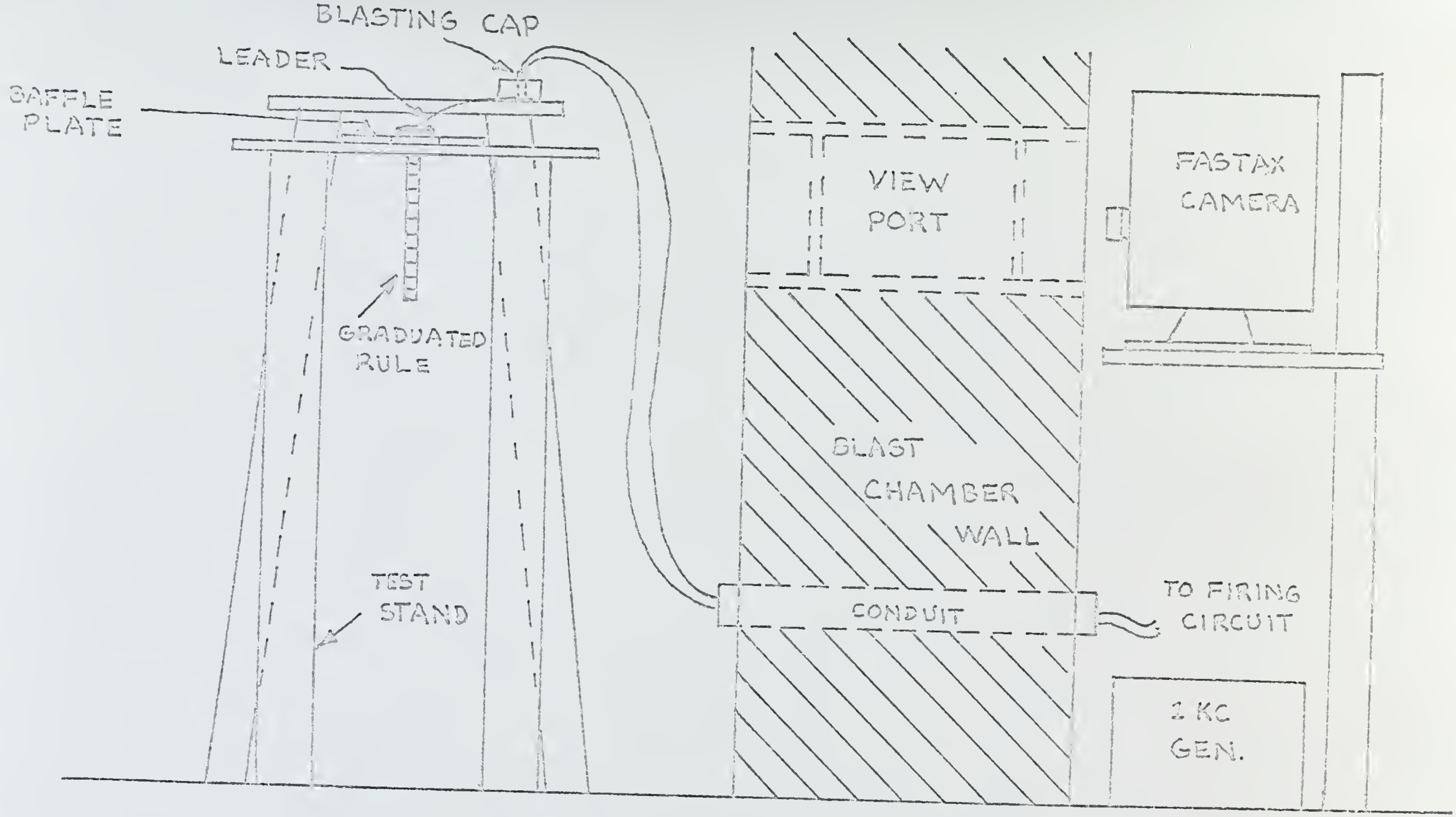

ARRANGEMENT OF APPARATUS FOR CALIBRATION TESTS

FIGURE B-1

Thesis 127272
G674 Grassit
Dynamic plastic behavior of intersecting shells.